Biofilms in porous media: Development of macroscopic transport equations via volume averaging with closure for local mass equilibrium conditions

Fabrice Golfier [a], Brian D. Wood [b,*], Laurent Orgogozo [a], Michel Quintard [c], Michel Buès [a]

[a] *Laboratoire Environnement, Géomécanique et Ouvrages, École Nationale Supérieure de Géologie, Nancy Université, Rue du Doyen Marcel Roubault, BP 40, F-54501 Vandœuvre-lès-Nancy, France*
[b] *School of Chemical, Biological, and Environmental Engineering, Oregon State University, Corvallis, OR 97331, United States*
[c] *Institut de Mécanique des Fluides, Allée du Professeur Camille Soula, 31400 Toulouse, France*

A B S T R A C T

In this work, we upscale a pore-scale description of mass transport in a porous medium containing biofilm to develop the relevant Darcy-scale equations. We begin with the pore-scale descriptions of mass transport, interphase mass transfer, and biologically-mediated reactions; these processes are then upscaled using the method of volume averaging to obtain the macroscale mass balance equations. We focus on the case of local mass equilibrium conditions where the averaged concentrations in the fluid and biological phases can be assumed to be proportional and for which a one-equation macroscopic model may be developed. We predict the effective dispersion tensor by a closure scheme that is solved for the cases of both simple and complex unit cells. The domain of validity of the approach is clearly identified, both theoretically and numerically, and unitless groupings indicating the domain of validity are reported.

Keywords:
Biofilm
Dispersion
Local mass equilibrium
Averaging
Homogenization

1. Introduction

The study of biofilms in porous media have had a long history from the environmental engineering perspective (e.g. [81]), and more recently have been of interest in applications to bioremediation in subsurface systems (e.g. [6–8,10,54,61,64,74]). A number of Darcy-scale mathematical models for describing the transport of biologically reactive dissolved solutes have been proposed. The literature on this topic is extensive, but summaries of the primary contributions in this area can be found in de Blanc et al. [14], and the review articles by Murphy and Ginn [38] and Ginn et al. [18]. Varying levels of sophistication in describing the underlying mechanisms have been attempted, but most models have been developed by first hypothesizing the important mass transfer and reaction processes involved, and then heuristically formulating the mathematical model at the Darcy scale by mass balancing. Thus, Darcy-scale parameters are assumed to exist and to be known *a priori* in such a formulation.

Developing the macroscale mass balance equations through a formal upscaling process [23,70] has become more familiar to hydrologists as we attempt to come to grips with the complexity and uncertainty in natural (and engineered) systems. The development of the effective dispersion tensor for heterogeneous subsurface systems is possibly the most successful and familiar example. Heterogeneous subsurface systems can be hierarchical not only in physical structure, but also in the combination of the physical, chemical, and biological processes that influence the transport of chemical species in the subsurface [11,12,70]. In Fig. 1, we have illustrated an example of the levels of heterogeneity possible in a subsurface (or engineered) system that involves microbial biofilms. These heterogeneities are characterized by a series of length-scales that range from the small length-scale associated with a representative volume of biofilm (Level I) to the large length-scale associated with applications, such as a bioreactor or bioremediation in the subsurface (Level III). We have assumed that the length-scales in a hierarchical heterogeneous porous medium system are disparate so that they may be represented discretely as indicated in the figure. At Level III, the characteristic length scale might be the size of the reactor or the size of subsurface heterogeneities characterizing spatial variations of the geological materials that comprise the aquifer. In general, these different geological materials may have different chemical, biological, and mechanical properties. At Level II, we have illustrated the solid and fluid that make up a representative elementary volume (REV) of the porous medium, and we have shown the microbes attached to the solids as a continuum phase. At Level I, we illustrate the multiphase nature of the microbial mass attached to the solid phase at the averaging volume scale of the biofilm; at this level, we treat the microbial phase itself as a two-phase system consisting of the intercellular region (the σ-phase) and the extracellular region including the extracellular polymeric substances (the β-phase).

* Corresponding author. Fax: +1 541 737 3099.
E-mail address: brian.wood@oregonstate.edu (B.D. Wood).

doi:10.1016/j.advwatres.2008.11.012

Nomenclature

Roman Letters

$A_{\gamma\kappa}$ interfacial area of the interface between the fluid and solid phases in an averaging volume or unit cell (m^2)

$A_{\gamma\omega}(t)$ interfacial area of the interface between the fluid and biofilm phases in an averaging volume or unit cell (m^2)

$A_{\omega\kappa}(t)$ interfacial area of the interface between the biofilm and solid phases in an averaging volume or unit cell (m^2)

$A_{\gamma e}$ the area associated with the γ-region at the boundaries of the unit cell, (m^2)

$A_{\omega e}$ the area associated with the ω-region at the boundaries of the unit cell, (m^2)

$\mathbf{b}_{A\gamma}$ closure variable that relates $\tilde{c}_{A\gamma}$ to sources involving $\nabla\langle c_{A\gamma}\rangle^{\gamma}$; defined by Eq. (46), ($m$)

$\mathbf{b}_{A\omega}$ closure variable that relates $\tilde{c}_{A\omega}$ to sources involving $\nabla\langle c_{A\omega}\rangle^{\omega}$; defined by Eq. (47), ($m$)

$\mathbf{b}'_{A\gamma}$ dimensionless form of the closure variable $\mathbf{b}_{A\gamma}$; defined by Eq. (58), (-)

$\mathbf{b}'_{A\omega}$ dimensionless form of the closure variable $\mathbf{b}_{A\omega}$; defined by Eq. (58), (-)

$\langle C_A\rangle$ superficial average concentration of species A per unit volume of the porous medium, as given by Eq. (21), (kg/m^3)

$\{c_A\}$ equilibrium weighted average concentration of species A, as given by Eq. (23), (kg/m^3)

$c_{A\gamma}$, $c_{B\gamma}$ mass concentration of species A or B (associated with volume V_d in Fig. 1) in the fluid phase (γ-region) (kg/m^3)

$c_{A\omega}$, $c_{B\omega}$ mass concentration of species A or B (associated with volume V_d in Fig. 1) in the biofilm phase (ω-region) (kg/m^3)

$\langle c_{A\gamma}\rangle, \langle c_{B\gamma}\rangle$ superficial average concentration of species A or B, as given by Eq. (9), (kg/m^3)

$\langle c_{A\gamma}\rangle^{\gamma}, \langle c_{B\gamma}\rangle^{\gamma}$ intrinsic average concentration of species A or B, as given by Eq. (11), (kg/m^3)

$\langle c_{A\omega}\rangle, \langle c_{B\omega}\rangle$ superficial average concentration of species A or B, as given by Eq. (8), (kg/m^3)

$\langle c_{A\omega}\rangle^{\omega}, \langle c_{B\omega}\rangle^{\omega}$ intrinsic average concentration of species A or B, as given by Eq. (12), (kg/m^3)

$\tilde{c}_{A\gamma}$ $= c_{A\gamma} - \langle c_{A\gamma}\rangle^{\gamma}$, Darcy scale deviation concentration in the fluid (γ-region) (kg/m^3)

$\tilde{c}_{\omega}$ $= c_{A\omega} - \langle c_{A\omega}\rangle^{\omega}$, Darcy scale deviation concentration in the biofilm (ω-region) (kg/m^3)

c_0 injected concentration in the nodular system, defined by Eq. (66) (kg/m^3)

C_{xx} spatially stationary covariance function for the indicator function of the γ-phase, (-)

Da_A $= \mu_{A\omega}\rho_{\omega}\ell_{\gamma}^2/K_{A\omega}\mathbf{D}_{A\gamma}$, a Damköhler number associated to the species A, (-)

$\mathrm{D}_{A\gamma}, \mathrm{D}_{B\gamma}$ molecular diffusion coefficient for the species A or B in the fluid, (m^2/s)

$D_{eff.\eta}$ Darcy scale (associated with volume V_d in Fig. 1) effective diffusion coefficient for solute in the matrix (η-region), (m^2/s)

$\mathbf{D}_{A\omega}, \mathbf{D}_{B\omega}$ effective diffusion tensor for species A or B in the biofilm (ω-region), (m^2/s)

$\mathbf{D}^*_{A.eff}$ Darcy scale (associated with volume $\mathscr{V}$ in Fig. 1) effective dispersion tensor for the substrate A, (m^2/s)

$\mathbf{D}^*_{A,xx}$ xx-component of the Darcy scale effective dispersion tensor $\mathbf{D}^*_{A,eff}$, (m^2/s)

$\mathbf{D}_{\Gamma}$ dimensionless effective diffusion tensor for species A (ω-region), defined by Eq. (60) (m^2/s)

$f_{A\gamma}$, $f_{A\omega}$ unclosed vectors defining the hydrodynamic dispersive flux, given by Eqs. (34) and (35), ($kg/m^2/s$)

I_{xx} integral scale associated to the γ-phase, defined by Eq. (64) (m)

$K_{A,eq}$ equilibrium partitioning coefficient between the fluid and biofilm phases for the species A, (-)

$K_{B,eq}$ equilibrium partitioning coefficient between the fluid and biofilm phases for the species B, (-)

$K_{A\omega}$ half-saturation constant for the substrate A, (-)

$K_{B\omega}$ half-saturation constant for the electron acceptor B, (-)

$\ell_{\eta}, \ell_{\omega}$ characteristic lengths associated with the Darcy scale (see Fig. 2), (m)

$\ell_{\gamma\omega}$ characteristic length associated with the Darcy scale, given by Eq. (32) (m)

L characteristic length associated with the macroscale averaging volume (see Fig. 1, Level III), (m)

ℓ_i lattice vector for the ith direction (i=l,2,3), (m)

$\mathbf{n}_{\gamma\kappa}$ $= -\mathbf{n}_{\kappa\gamma}$, unit normal vector, pointing from the γ-phase toward the κ-phase, (-)

$\mathbf{n}_{\gamma\omega}$ $= -\mathbf{n}_{\omega\gamma}$, unit normal vector, pointing from the γ-phase toward the ω-phase, (-)

$\mathbf{n}_{\omega\kappa}$ $= -\mathbf{n}_{\kappa\omega}$, unit normal vector, pointing from the ω-phase toward the κ-phase, (-)

Pe_A $= \|v_{\gamma}\|\ell_{\gamma}/\mathbf{D}_{A\gamma}$, a Péclet number associated to the species A, (-)

r_0 characteristic length associated with a biofilm-scale averaging volume (Fig. 1, Level I), (m)

R_0 characteristic length associated with the Darcy-scale averaging volume (Fig. 2), (m)

$R_{A\omega}$ nonlinear Monod kinetic reaction term, defined by Eq. (7), ($kg/m^3/s$)

$\langle R_{A\omega}\rangle^{\omega}$ intrinsic average of the reaction term in the ω-phase, defined by Eq. (18), ($kg/m^3/s$)

$\langle R_{A\omega}\rangle^{\omega}$ average reaction rate, defined by Eq. (36), ($kg/m^3/s$)

$\mathbf{v}_{\gamma}$ pore scale fluid velocity vector, (m/s)

$\langle\mathbf{v}_{\gamma}\rangle^{\gamma}$ intrinsic average fluid velocity vector, (m/s)

$\tilde{\mathbf{v}}_{\gamma}$ $= \mathbf{v}_{\gamma} - \langle\mathbf{v}_{\gamma}\rangle^{\gamma}$, fluid velocity deviation vector for the fluid, (m/s)

$\mathscr{V}$ volume associated with a Darcy scale averaging volume, as defined in Fig. 1, (m^3)

$\mathscr{V}_M$ volume associated with a macroscale averaging volume, as defined in Fig. 1, (m^3)

$\mathscr{V}_{micro}$ volume associated with a biofilm scale averaging volume, as defined in Fig. 1, (m^3)

V_{γ} volume associated with the fluid within an averaging volume, (m^3)

V_{κ} volume associated with the solid within an averaging volume, (m^3)

V_{ω} volume associated with the biofilm within an averaging volume, (m^3)

Greek Letters

β phase indicator for the extracellular polymeric substances associated with the averaging volume scale of the biofilm (Level I of Fig. 1), (-)

γ phase indicator for the fluid associated with the representative elementary volume of the porous medium (Level II of Fig. 1), (-)

δ power-law exponent expressing the Péclet number-dependence of the longitudinal dispersion coefficient, (-)

ε_{γ} $= V_{\gamma}(t)/\mathscr{V}$, the volume fraction of the fluid phase, (-)

ε_{κ} $= V_{\kappa}/\mathscr{V}$, the volume fraction of the solid phase, (-)

ε_{ω} $= V_{\omega}(t)/\mathscr{V}$, the volume fraction of the biofilm, (-)

κ phase indicator for the solid associated with the representative elementary volume of the porous medium (Level II of Fig. 1), (-)

$\mu_{A\omega}$ specific degradation rate for the substrate *A*, (1/s)

$\mu_{B\omega}$ specific degradation rate for the electron acceptor *B*, (1/s)

ρ_{ω} microbial concentration *(kg/m^3)*

σ phase indicator for the intercellular region associated with the averaging volume scale of the biofilm (Level I of Fig. 1), (-)

$\Psi_{\gamma}(\mathbf{x})$ indicator function for the γ-phase, defined by Eq. (65)

ω phase indicator for the biofilm associated with the representative elementary volume of the porous medium (Level II of Fig. 1), (-)

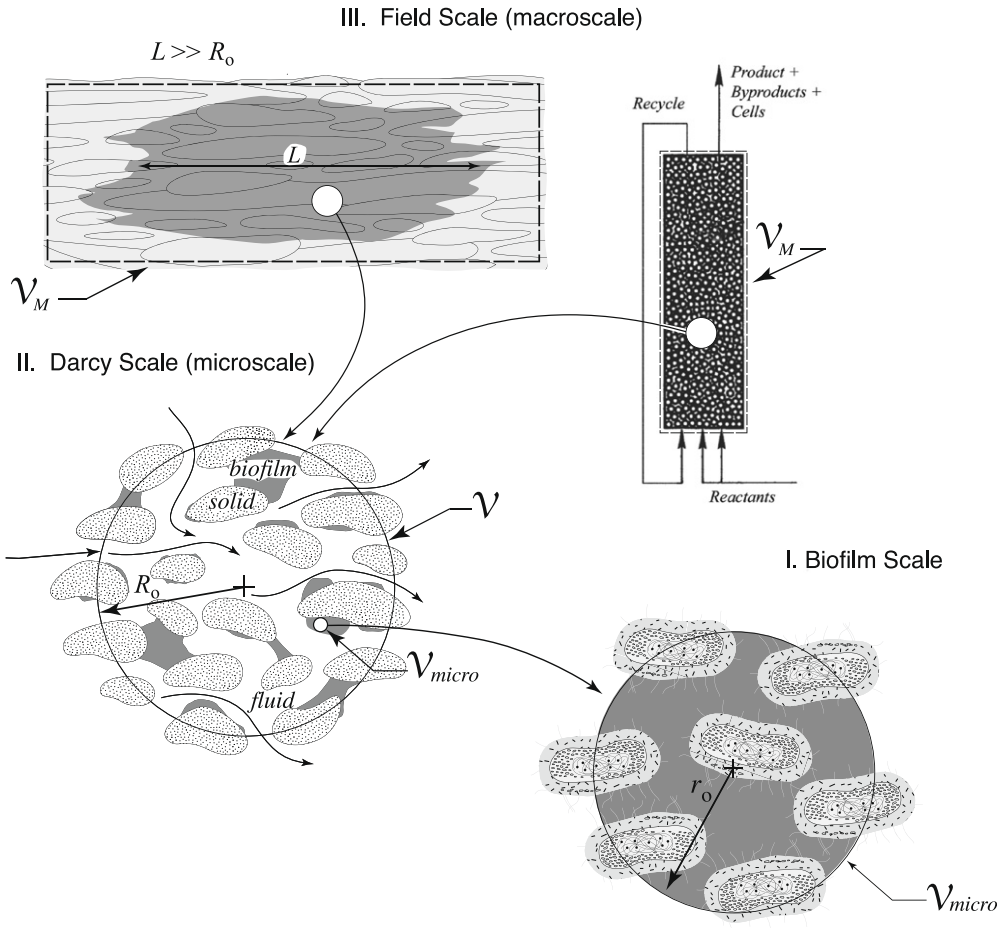

Fig. 1. An example of hierarchy of scales associated with the biodegradation of aqueous species.

The details of upscaling from the cell scale to the biofilm scale (Level I) have been developed previously [71–73,75].

In this work, we continue this study by upscaling from the microscale, characterized by discrete fluid and biofilm phases (of which properties have been upscaled from the lower scale), with characteristic lengths ℓ_γ and ℓ_ω, respectively, to the Darcy scale (Level II), characterized by the length scale R_0. The various length scales associated with Level II are illustrated in Fig. 2.

For cases where the biological phase can be treated as a well-defined continuum, one can identify three potentially important regimes and hence three distinct transport models that describe the mass transfer and reaction processes within the biofilms: (1) a *one-equation local mass equilibrium* regime [29,77,78] where the averaged concentrations of chemical species in the fluid and biofilm can be assumed to be in equilibrium (cf. the *local mass equilibrium assumption* described by Valocchi [65]), (2) a *one-equation non-equilibrium* regime, where spatial gradients may exist only in one of both phases and the reaction can be assumed to be limited by mass transfer or kinetics so that a one-equation model can still be developed through the identification of a macroscopic-scale effectiveness factor or mass exchange coefficient between phases [15,52], and (3) a *two-equation non-equilibrium* regime where the averaged concentrations in the two phases are not in equilibrium, and the resulting description must involve two separate conservation equations (one for the biofilm phase and one for the fluid phase). Each of these models induces some limitations and constraints but all of them will ultimately be necessary if one wants to describe macroscopic-scale chemical transport and transformation in porous media under all conditions. For the purposes of this work we will focus our efforts on the one-equation equilibrium model.

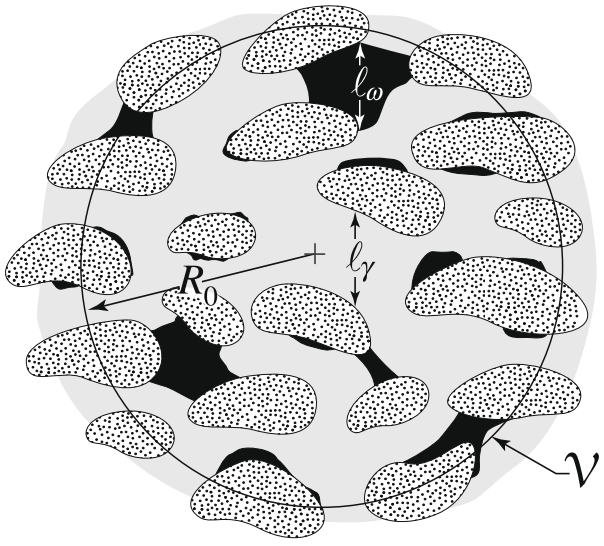

Fig. 2. Definition of the phases associated to the averaging volume (Darcy-scale).

Although mass balance equations are often posed heuristically for describing biological processes in porous media, it is sometimes unclear exactly what is meant by each of the parameters that ap-

pear in these equations. Moreover, the question of the validity of such equations is rarely raised. Few studies to date have attempted to formally upscale or homogenize the equations describing mass transport, mass transfer, and reactions that apply at the pore scale to develop a Darcy-scale description. Two notable exceptions are the works by Dykaar and Kitanidis [15] and Knutson et al. [28]. Dykaar and Kitanidis [15] used a Taylor–Aris moment approach to compute the effective dispersion tensor and effective reaction rate for the solute biodegradation in porous media. These results were for a two-dimensional sinusoidal pore geometry. More recently, Knutson et al. [28] determined the effective transverse dispersion coefficient from pore-scale simulations on a two-dimensional staggered array of cylinders. They observed a difference of up to 50% in the dispersion tensor components between the passive and reactive cases. Their work was limited to a scenario of transverse mixing where the biofilm growth is restricted to a small part of the pore space.

The specific goals of this work are to: (1) use volume averaging to develop the macroscale mass balance equations transport of an electron donor and an electron acceptor undergoing biodegradation in a porous medium; (2) define how the macroscopic effective parameters relate to the sub-pore scale processes (which might be measured in a laboratory batch system), and (3) determine the associated domain of validity of such a model through a comparison with direct pore-scale simulations in terms of characteristic dimensionless numbers of the process.

2. Upscaling the microscale description of biofilms in porous media

2.1. Microscale model

We begin this investigation by introducing the set of mass balance equations that are used for describing conservation of mass at the sub-pore scale (Fig. 2) in the fluid (γ-phase) and the biofilm (ω-phase). The description of the biofilm as a continuum phase has been described previously by Wood and Whitaker [71,73]. Note that in these equations a convection term does not appear in the biofilm phase because connected fluid pathways where convection occurs are technically part of the fluid phase. If the fluid pathways in the biofilm phase were very small compare to the Darcy-scale pore size, an intermediate upscaling for such channelled biofilms might be necessary. Such a case is beyond the scope of this study, but it has been considered recently by Aspa et al. [4].

The set of conservation equations for the fluid–biofilm–solid system takes the following form (which is consistent with a number of previous studies on biofilms, e.g. [17,76]).

2.1.1. Biofilm phase

$$\frac{\partial c_{A\omega}}{\partial t} = \nabla\cdot(\mathbf{D}_{A\omega}\cdot\nabla c_{A\omega}) + R_{A\omega} \quad \text{in the } \omega\text{-phase}, \tag{1}$$

$$\text{B.C.1} \qquad -\mathbf{n}_{\omega\kappa}\cdot\mathbf{D}_{A\omega}\cdot\nabla c_{A\omega} = 0 \quad \text{at } A_{\omega\kappa}(t), \tag{2}$$

$$\text{B.C.2} \qquad -\mathbf{n}_{\gamma\kappa}\cdot\mathbf{D}_{A\gamma}\nabla c_{A\gamma} = 0 \quad \text{at } A_{\gamma\kappa}, \tag{3}$$

$$\text{B.C.3} \qquad c_{A\gamma} = K_{A,eq}c_{A\omega} \quad \text{at } A_{\gamma\omega}(t), \tag{4}$$

$$\text{B.C.4} \qquad -\mathbf{n}_{\gamma\omega}\cdot\mathbf{D}_{A\omega}\cdot\nabla c_{A\omega} = -\mathbf{n}_{\gamma\omega}\cdot\mathscr{D}_{A\gamma}\nabla c_{A\gamma} \quad \text{at } A_{\gamma\omega}(t), \tag{5}$$

2.1.2. Fluid phase

$$\frac{\partial c_{A\gamma}}{\partial t} + \mathbf{v}_\gamma\cdot\nabla c_{A\gamma} = \nabla\cdot(\mathscr{D}_{A\gamma}\nabla c_{A\gamma}) \quad \text{in the } \gamma\text{-phase}. \tag{6}$$

Here, $c_{A\gamma}$ and $c_{A\omega}$ represent the mass concentration of species A (substrate) in the fluid and biofilm phases, respectively; $\mathscr{D}_{A\gamma}$ is the diffusion coefficient for the fluid and $\mathbf{D}_{A\omega}$ is the effective diffusion tensor for the biofilm; $\mathbf{v}_\gamma$ is the fluid velocity; $K_{A,eq}$ is the equilibrium partitioning coefficient between the fluid and biofilm phases; and $R_{A\omega}$ is a nonlinear kinetic reaction term. We have used the terminology $A_{\gamma\kappa}$ to indicate the surface area between the fluid and solid phases, and (similarly) $A_{\gamma\omega}(t)$ and $A_{\omega\kappa}(t)$ to indicate the surface area between the fluid and biofilm phases and between the biofilm and solid phases, respectively. The term $\mathbf{n}_{\gamma\kappa}$ indicates the unit normal pointing outward from the γ-phase toward the ω-phase; $\mathbf{n}_{\gamma\omega}$ and $\mathbf{n}_{\omega\kappa}$ are similarly defined. In principle, the volume of biofilm, $V_\omega(t)$, within the volume $\mathscr{V}$ changes in time due to the biofilm growth (or decay); hence all other parameters, such as $A_{\gamma\omega}(t)$, associated with this volume also change with time. This evolution of the microbial biomass phase within the porous medium is a complex process due mainly to growth and spatial spreading of the cellular phase. Processes such as biofilm sloughing and attachment (or detachment) of cells from the fluid phase may also contribute to the biofilm volume variation. Several models [63,26,57] have been formulated in the literature. They are usually based on a semi-empirical description although an upscaling leading to the macroscale equation for the biomass density in the biofilm was considered recently by Wood and Whitaker [72]. A commonly-adopted approach to this coupling is to utilize a quasi-steady assumption; this implies that the evolution of the system geometry occurs on a time scale large compared with the time scale for mass transfer processes [58,42]. This time-evolving interface problem is similar to the one encountered in dissolution/precipitation [20] or in combustion in porous media [25,44,33], to cite only those, for which the quasi-steady assumption is classically adopted.

For this analysis, we have focused on systems with a single substrate (carbon and energy source) which has been denoted as species A, and a single electron acceptor (such as oxygen) which has been denoted as species B. We have adopted the dual-Monod form [32] for the reaction term

$$R_{A\omega} = -\mu_{A\omega}\rho_\omega\frac{c_{A\omega}}{c_{A\omega}+K_{A\omega}}\frac{c_{B\omega}}{c_{B\omega}+K_{B\omega}}, \tag{7}$$

where $\mu_{A\omega}$ is the specific degradation rate for the substrate; ρ_ω is the microbial concentrations; $K_{A\omega}$, and $K_{B\omega}$ are the half-saturation constants for the substrate and electron acceptor, respectively; and $c_{B\omega}$ is the mass concentration of electron acceptor in the biofilm phase. In principle, the nutrient consumption rate is determined by local conditions in the biofilm and may depend explicitly on time or space. Although there are a wide variety of substrate uptake and growth models in the literature (e.g. [53,5,27]), the dual-Monod form is the most commonly-adopted model because it correctly represents the main physical mechanisms but staying simple mathematically [6].

Because the biofilm is itself a multiphase system consisting of cells and extracellular material, it is necessary to be very specific about what is intended by the concentrations $c_{A\omega}$, $c_{B\omega}$, and ρ_ω. In this case, $c_{A\omega}$, $c_{B\omega}$ are most conveniently interpreted as spatial average concentrations, and ρ_ω is interpreted as a superficial volume average. Interested readers can refer to Wood and Whitaker [73] and Wood et al. [75] for more details about the development of Eqs. (1)–(7). Note that a similar set of conservation equations also holds for species B, but since the analysis is similar to that for species A, we will not explicitly derive them here.

2.2. Development of the averaged equations

Referring to the averaging volume, $\mathscr{V}$, illustrated in Fig. 2, we define the *superficial average* concentration of species A in the ω-phase (biofilm) as

$$\langle c_{A\omega}\rangle = \frac{1}{\mathscr{V}}\int_{V_\omega(t)} c_{A\omega}\,dV. \tag{8}$$

Here, $\mathscr{V}$ represents the averaging volume shown in Fig. 2, and $V_\omega(t)$ represents the volume of the ω-phase contained in the averaging volume. A similar definition holds for the average concentration of species A in the γ-phase,

$$\langle c_{A\gamma}\rangle = \frac{1}{\mathscr{V}}\int_{V_\gamma(t)} c_{A\gamma}\, dV. \tag{9}$$

Often, in applications, it is preferable to work with a concentration that represents the average over the pore space rather than the total volume of the porous medium. This concentration is the *intrinsic average* concentration, and for the two averages defined above the intrinsic averages are given by

$$\langle c_{A\omega}\rangle^{\omega} = \frac{1}{V_\omega(t)}\int_{V_\omega(t)} c_{A\omega}\, dV, \tag{10}$$

$$\langle c_{A\gamma}\rangle^{\gamma} = \frac{1}{V_\gamma(t)}\int_{V_\gamma(t)} c_{A\gamma}\, dV. \tag{11}$$

The intrinsic and superficial averages are related through the volume fractions of the two phases as follows:

$$\langle c_{A\omega}\rangle = \varepsilon_\omega \langle c_{A\omega}\rangle^{\omega}, \tag{12}$$

$$\langle c_{A\gamma}\rangle = \varepsilon_\gamma \langle c_{A\gamma}\rangle^{\gamma}, \tag{13}$$

where ε_ω and ε_γ represent the volume fractions of the ω- and γ-phases, respectively, such that $\varepsilon_\gamma + \varepsilon_\omega + \varepsilon_\kappa = 1$.

In the developments that follow, we will make use of the spatial decompositions in order to remove averaged quantities from point values

$$c_{A\omega} = \langle c_{A\omega}\rangle^{\omega} + \tilde{c}_{A\omega}, \tag{14}$$

$$c_{A\gamma} = \langle c_{A\gamma}\rangle^{\gamma} + \tilde{c}_{A\gamma}. \tag{15}$$

The process of volume averaging is initiated by forming the superficial average of phase conservation equations (1)–(7). In order to interchange the time derivative and averaging operation, one must make use of the general transport theorem [69], while for the first term the spatial averaging theorem [21,24] is required. As emphasized previously, the geometry of the biofilm (as represented by $V_\omega(t)$), may evolve in time due to the biofilm growth, decay, sloughing, or accretion. However, given the large difference between characteristic time scales for growth and for solute transport (cf. [58,42]), movement of the fluid–biofilm interface due to biofilm growth can be usually neglected relative to the rate of diffusive transport. In this work, we have thus explicitly adopted the approximation that mass transport due to the velocity, **w**, of the fluid–biofilm interface can be neglected relative to the rates of mass transport by diffusion [71]. This quasi-steady approximation serves to uncouple the transport process from the biofilm growth process. By introducing the assumption of a time-invariant microbial population, kinetic parameters and pore-scale geometry are kept constant. Results obtained this way would apply only to a particular biofilm configuration. In principle, one could include the effects of an evolving biofilm geometry by introducing one or more additional macroscopic equations describing the growth, decay and attachment/detachment of the biofilm phase.

The complete development for averaging equations (1)–(7) is available in Appendix A, and the result is

Averaged equation for the biofilm (ω-phase)

$$\underbrace{\frac{\partial(\varepsilon_\omega\langle c_{A\omega}\rangle^{\omega})}{\partial t}}_{\text{Accumulation}} = \underbrace{\nabla\cdot\left[\varepsilon_\omega \mathbf{D}_{A\omega}\cdot\left(\nabla\langle c_{A\omega}\rangle^{\omega} + \frac{1}{V_\omega}\int_{A_{\omega\gamma}(t)}\mathbf{n}_{\omega\gamma}\tilde{c}_{A\omega}\,dA + \frac{1}{V_\omega}\int_{A_{\omega\kappa}(t)}\mathbf{n}_{\omega\kappa}\tilde{c}_{A\omega}\,dA\right)\right]}_{\text{Diffusion}}$$
$$+ \underbrace{\frac{1}{\mathscr{V}}\int_{A_{\omega\gamma}(t)}\mathbf{n}_{\omega\gamma}\cdot(\mathbf{D}_{A\omega}\cdot\nabla c_{A\omega})dA + \frac{1}{\mathscr{V}}\int_{A_{\omega\kappa}(t)}\mathbf{n}_{\omega\kappa}\cdot(\mathbf{D}_{A\omega}\cdot\nabla c_{A\omega})dA}_{\text{Interfacial Flux}} + \underbrace{\varepsilon_\omega\langle R_{A\omega}\rangle^{\omega}}_{\text{Reaction}}, \tag{16}$$

Averaged equation for the fluid (γ-phase)

$$\underbrace{\frac{\partial(\varepsilon_\gamma\langle c_{A\gamma}\rangle^{\gamma})}{\partial t}}_{\text{Accumulation}} + \underbrace{\nabla\cdot(\varepsilon_\gamma\langle \mathbf{v}_\gamma\rangle^{\gamma}\langle c_{A\gamma}\rangle^{\gamma})}_{\text{Convection}} = \underbrace{\nabla\cdot\left[\varepsilon_\gamma \mathbf{D}_{A\gamma}\left(\nabla\langle c_{A\gamma}\rangle^{\gamma} + \frac{1}{V_\gamma}\int_{A_{\omega\gamma}(t)}\mathbf{n}_{\gamma\omega}\tilde{c}_{A\gamma}\,dA + \frac{1}{V_\gamma}\int_{A_{\omega\kappa}(t)}\mathbf{n}_{\gamma\kappa}\tilde{c}_{A\gamma}\,dA\right)\right]}_{\text{Diffusion}}$$
$$+ \underbrace{\frac{1}{\mathscr{V}}\int_{A_{\omega\gamma}(t)}\mathbf{n}_{\gamma\omega}\cdot(\mathbf{D}_{A\gamma}\nabla c_{A\gamma})dA + \frac{1}{\mathscr{V}}\int_{A_{\omega\kappa}(t)}\mathbf{n}_{\gamma\kappa}\cdot(\mathbf{D}_{A\gamma}\nabla c_{A\gamma})dA}_{\text{Interfacial Flux}} - \underbrace{\nabla\cdot\langle\tilde{v}_\gamma\tilde{c}_{A\gamma}\rangle}_{\text{Dispersive Transport}}. \tag{17}$$

The quantities $\tilde{c}_{A\omega}$ and $\tilde{c}_{A\gamma}$ are referred to as spatial deviation concentrations. Again, we note that relations analogous to Eqs. (14) and (15) also hold for species B.

In Eq. (16), we have used the following relationship (cf. the parallel development of the reaction term at the biofilm scale described in [73, Appendix A]), which holds for $\ell_\gamma, \ell_\omega \ll R_0$,

$$\langle R_{A\omega}\rangle^{\omega} = -\mu_{A\omega}\rho_{\omega}\frac{\langle c_{A\omega}\rangle^{\omega}}{\langle c_{A\omega}\rangle^{\omega}+K_{A\omega}}\frac{\langle c_{B\omega}\rangle^{\omega}}{\langle c_{B\omega}\rangle^{\omega}+K_{B\omega}}. \tag{18}$$

Additional details about the averaging process are available in Appendix A.

3. Local mass equilibrium

3.1. The one-equation model

When biofilms are present in porous media there exists an essentially immobile phase in which chemical species can be entrained via diffusion. For the most general description of transport at the Darcy scale, one would expect that at least a two-equation model would be necessary. However, when the characteristic time for transport in the fluid phase is of the same order of magnitude as the characteristic time for diffusion within the biofilm and the characteristic time associated to the reaction kinetics is large, it is also possible to imagine a second regime in which a one-equation local mass equilibrium model might be a reasonable approximation. In this section, we develop such a model and present some constraints that indicate the conditions for which a one-equation equilibrium model is valid.

3.1.1. Local mass equilibrium

Under conditions of *thermodynamic equilibrium*, i.e., zero concentration gradients, the equilibrium relationship established only at the fluid–biofilm interface by Eq. (4) can be extended to the entire domain and we obtain

$$\langle c_{A\gamma}\rangle^{\gamma} = K_{A,eq}\langle c_{A\omega}\rangle^{\omega} \quad \text{at thermodynamic equilibrium.} \tag{19}$$

Even when the condition of thermodynamic equilibrium does not exist, Eq. (19) can be used as a reasonable approximation if the system behaviour is close to the equilibrium. When this occurs, we say that the condition of *local mass equilibrium* [65,71,73] is valid. It must be emphasized that the local mass equilibrium assumption does not imply a zero gradient everywhere, as ideally assumed in Eq. (19), *but a situation close to this condition*, i.e., small macroscale concentration gradients both in the fluid and biofilm phases. Under these circumstances, the concentrations predicted by Eqs. (16) and (17) are tied to one another, and these equations can be added together to produce a one-equation expression describing solute transport. Adding these equations eliminates the interfacial flux terms [through the boundary condition given by Eq. (5)] and yields a single equation of the form

$$\begin{aligned}
&\frac{\partial}{\partial t}\left(\varepsilon_{\omega}\langle c_{A\omega}\rangle^{\omega}+\varepsilon_{\gamma}\langle c_{A\gamma}\rangle^{\gamma}\right)+\nabla\cdot\left(\varepsilon_{\gamma}\langle \mathbf{v}_{\gamma}\rangle^{\gamma}\langle c_{A\gamma}\rangle^{\gamma}\right)\\
&\quad=\nabla\cdot\left[\mathbf{D}_{A\omega}\cdot\left(\varepsilon_{\omega}\nabla\langle c_{A\omega}\rangle^{\omega}+\frac{1}{\mathscr{V}}\int_{A_{\omega\gamma}(t)}\mathbf{n}_{\omega\gamma}\tilde{c}_{A\omega}\,dA\right.\right.\\
&\qquad+\frac{1}{\mathscr{V}}\int_{A_{\omega\kappa}(t)}\mathbf{n}_{\omega\kappa}\tilde{c}_{A\omega}\,dA\Big)+\mathscr{D}_{A\gamma}\left(\varepsilon_{\gamma}\nabla\langle c_{A\gamma}\rangle^{\gamma}+\frac{1}{\mathscr{V}}\int_{A_{\omega\gamma}(t)}\mathbf{n}_{\gamma\omega}\tilde{c}_{A\gamma}\,dA\right.\\
&\qquad\left.\left.+\frac{1}{\mathscr{V}}\int_{A_{\omega\kappa}(t)}\mathbf{n}_{\gamma\kappa}\tilde{c}_{A\gamma}\,dA\right)\right]-\nabla\cdot\langle\tilde{\mathbf{v}}_{\gamma}\tilde{c}_{A\gamma}\rangle+\varepsilon_{\omega}\langle R_{A\omega}\rangle^{\omega}.
\end{aligned}\tag{20}$$

Although the macroscale transport equation above represents a one-equation model, it is still not in the form that is conventionally used to describe mass transport in biofilms. In order to put this expression in the conventional form of a one-equation convection–dispersion–reaction model, we need to accomplish two things: (1) the spatial deviation concentrations need to be eliminated by expressing them in terms proportional to the volume averaged concentrations (through the closure problem, described furthering Section 4), and (2) we need to define a single concentration that characterizes the system at equilibrium. These are discussed in the material following.

3.1.2. Spatial average and equilibrium weighted concentrations

For a system in which there are two phases in which chemical species reside, the following *spatial average* concentration could be used

$$\langle c_A\rangle \equiv \frac{1}{\mathscr{V}}\int_{\mathscr{V}} c_A\,dV = \varepsilon_{\gamma}\langle c_{A\gamma}\rangle^{\gamma}+\varepsilon_{\omega}\langle c_{A\omega}\rangle^{\omega}. \tag{21}$$

In this definition, $\langle c_A\rangle$ corresponds here to the mass of species A per unit volume of the porous medium. The advantage to this formulation is that it corresponds more closely to the concentration that might be measured by most of experimental methods.

At *equilibrium*, the spatial average concentration is given by [using Eq. (19)]

$$\langle c_A\rangle = [\varepsilon_{\gamma}+\varepsilon_{\omega}K_{A,eq}^{-1}]\langle c_{A\gamma}\rangle^{\gamma}. \tag{22}$$

One could make use of this spatial average concentration in order to develop a one-equation model. However, it is difficult to define constraints indicating the conditions for validity of the one-equation model on the basis of this definition. To find these constraints, we propose an *equilibrium weighted average* concentration (e.g. [39,71,73]) given by

$$\{c_A\} \equiv \left(\frac{\varepsilon_{\gamma}}{\varepsilon_{\omega}+\varepsilon_{\gamma}}\right)\langle c_{A\gamma}\rangle^{\gamma}+\left(\frac{\varepsilon_{\omega}}{\varepsilon_{\omega}+\varepsilon_{\gamma}}\right)K_{A,eq}\langle c_{A\omega}\rangle^{\omega}. \tag{23}$$

For this definition, note that from Eqs. (22) and (23) at thermodynamic equilibrium we have the equivalences

$$\langle c_{A\gamma}\rangle^{\gamma} = K_{A,eq}\langle c_{A\omega}\rangle^{\omega} = \frac{\langle c_A\rangle}{(\varepsilon_{\gamma}+\varepsilon_{\omega}K_{A,eq}^{-1})} = \{c_A\}$$
$$\text{at thermodynamic equilibrium.} \tag{24}$$

Once local mass equilibrium is established, the final conservation equation can be expressed in terms of any of the concentrations (equilibrium weighted average, spatial average, or extracellular intrinsic average) appearing in Eq. (24).

3.1.3. Constraints for local mass equilibrium

If conditions of thermodynamic equilibrium were to exist, we could use Eq. (24) directly to express Eq. (20) entirely in terms of the equilibrium weighted concentration. However, for a system in which transport is occurring, thermodynamic equilibrium cannot be achieved exactly. Instead, we seek to find the conditions for which we are close enough to equilibrium so that the assumption of local mass equilibrium is valid. To develop constraints that indicate under what conditions local mass equilibrium is valid approximation, we first note that near equilibrium Eq. (24) is not exactly correct, but must be expressed in the form

$$\langle c_{A\gamma}\rangle^{\gamma} = \{c_A\}+\hat{c}_{A\gamma}, \tag{25}$$
$$K_{A,eq}\langle c_{A\omega}\rangle^{\omega} = \{c_A\}+\hat{c}_{A\omega}, \tag{26}$$

where $\hat{c}_{A\gamma}$ and $\hat{c}_{A\omega}$ represent deviations of the local volume average concentrations (weighted by $K_{A,eq}$ for the biofilm phase) from the equilibrium weighted average. When these expressions are used in Eq. (20), one can show that the approximation of local mass equilibrium is valid when several restrictions are verified. The interested reader may refer to Wood et al. [78] for a presentation and analysis of these conditions. The restrictions can be expressed in terms of unitless parameter groupings of the problem such as the Damköhler and the Péclet numbers associated to the species A which are defined by

$$Da_A = \frac{\mu_{A\omega}\rho_\omega \ell_\gamma^2}{K_{A\omega}\mathscr{D}_{A\gamma}}, \tag{27}$$

$$Pe_A = \frac{\|\boldsymbol{v}_\gamma\|\ell_\gamma}{\mathscr{D}_{A\gamma}}. \tag{28}$$

Note that in Eq. (28) we have used the notation

$$\|\boldsymbol{v}_\gamma\| = (\langle \mathbf{v}_\gamma\rangle^\gamma \cdot \langle \mathbf{v}_\gamma\rangle^\gamma)^{\frac{1}{2}}, \tag{29}$$

and restrictions take the form [78]

$$\left(\frac{\varepsilon_\gamma\varepsilon_\omega}{\varepsilon_\gamma+\varepsilon_\omega}\right)\left(\frac{\mathscr{D}_{A\gamma}-\mathbf{D}_{A\omega}}{\mathbf{D}^*_{A,eff}}\right)\left(\frac{\ell_{\gamma\omega}}{L}\right)^2 \ll 1, \tag{30}$$

$$\left(\frac{\varepsilon_\gamma\varepsilon_\omega}{\varepsilon_\gamma+\varepsilon_\omega}\right)Da_A \ll 1, \tag{31}$$

$$\left(\frac{\varepsilon_\gamma\varepsilon_\omega}{\varepsilon_\gamma+\varepsilon_\omega}\right)\left(\frac{\ell_{\gamma\omega}}{L}\right)Pe_A \ll 1, \tag{32}$$

where $\ell^2_{\gamma\omega} = \delta a_v \varepsilon_\gamma\varepsilon_\omega/(\varepsilon_\gamma+\varepsilon_\omega)$, $D^*_{A,eff}$ is the effective dispersion tensor for the species A and δ represents a concentration boundary layer thickness in the fluid phase.

Note that these kinds of order-of-magnitude estimates should be used with caution. Such restrictions are usually more restrictive than needed due to simplifying assumptions required for their development. In addition, results obtained in the case of a purely diffusive problem [47] have shown that it may be difficult to catch geometrical effects through simple unitless groupings. Following this work, rather than estimating the theoretical domain validity associated to these conditions, we preferred to study the validity of our macroscopic model through a direct comparison between macroscopic approach and simulations at the lower scale. We will explore this point further in Section 6.

When these constraints are met, one can use the relationship given by Eq. (23) to express Eq. (20) entirely in terms of the equilibrium-weighted concentration, i.e.,

Macroscopic transport equation (unclosed).

$$\underbrace{\frac{\partial}{\partial t}((\varepsilon_\omega + K^{-1}_{A,eq}\varepsilon_\gamma)\{c_A\})}_{\text{Accumulation}} + \underbrace{\nabla\cdot(\varepsilon_\gamma\langle\mathbf{v}_\gamma\rangle^\gamma\{c_A\})}_{\text{Convection}} = \underbrace{\nabla\cdot[(\varepsilon_\gamma\mathscr{D}_{A\gamma}\mathbf{I} + K^{-1}_{A,eq}\varepsilon_\omega\mathbf{D}_{A\omega})\cdot\nabla\{c_A\}]}_{\text{Conventional Diffusion Term}} + \underbrace{\nabla\cdot[\mathbf{f}_{A\omega}+\mathbf{f}_{A\gamma}]}_{\text{Hydrodynamic Dispersion}} + \underbrace{\varepsilon_\omega\{R_{A\omega}\}}_{\text{Reaction}}. \tag{33}$$

Here $\mathbf{f}_{A\omega}$ and $\mathbf{f}_{A\gamma}$ are the unclosed vectors that define the hydrodynamic dispersive flux, given by

$$\mathbf{f}_{A\gamma} = \mathscr{D}_{A\gamma}\mathbf{I}\cdot\left(\frac{1}{\mathscr{V}}\int_{A_{\omega\gamma}(t)}\mathbf{n}_{\gamma\omega}\tilde{c}_{A\gamma}\,dA + \frac{1}{\mathscr{V}}\int_{A_{\omega\kappa}(t)}\mathbf{n}_{\gamma\kappa}\tilde{c}_{A\gamma}\,dA\right) - \nabla\cdot\langle\tilde{\mathbf{v}}_\gamma\tilde{c}_{A\gamma}\rangle, \tag{34}$$

$$\mathbf{f}_{A\omega} = \mathbf{D}_{A\omega}\cdot\left(\frac{1}{\mathscr{V}}\int_{A_{\omega\gamma}(t)}\mathbf{n}_{\omega\gamma}\tilde{c}_{A\omega}\,dA + \frac{1}{\mathscr{V}}\int_{A_{\omega\kappa}(t)}\mathbf{n}_{\omega\kappa}\tilde{c}_{A\omega}\,dA\right), \tag{35}$$

and $\{R_{A\omega}\}$ is the notation for the average reaction rate

$$\{R_{A\omega}\} = -\mu_{A\omega}\rho_\omega\frac{\{c_A\}}{\{c_A\}+K_{A,eq}K_{A\omega}}\frac{\{c_B\}}{\{c_B\}+K_{B,eq}K_{B\omega}}. \tag{36}$$

Note that, because the condition of local mass equilibrium applies, we have that $\langle c_{A\gamma}\rangle^\gamma = K_{A,eq}\langle c_{A\omega}\rangle^\omega = \{c_A\}$. Using these relations in the result above, we develop a more conventional form for the macroscale transport equation.

Macroscopic transport equation (unclosed), fluid-phase concentration form.

$$\underbrace{\frac{\partial}{\partial t}((\varepsilon_\omega + K^{-1}_{A,eq}\varepsilon_\gamma)\langle c_{A\gamma}\rangle^\gamma)}_{\text{Accumulation}} + \underbrace{\nabla\cdot(\varepsilon_\gamma\langle\mathbf{v}_\gamma\rangle^\gamma\langle c_{A\gamma}\rangle^\gamma)}_{\text{Convection}} = \underbrace{\nabla\cdot[(\varepsilon_\gamma\mathscr{D}_{A\gamma}\mathbf{I} + K^{-1}_{A,eq}\varepsilon_\omega\mathbf{D}_{A\omega})\cdot\nabla\langle c_{A\gamma}\rangle^\gamma]}_{\text{Conventionnal Diffusion Term}} + \underbrace{\nabla\cdot[\mathbf{f}_{A\omega}+\mathbf{f}_{A\gamma}]}_{\text{Hydrodynamic Dispersion}} - \underbrace{\varepsilon_\omega\mu_{A\omega}\rho_\omega\frac{\langle c_{A\gamma}\rangle^\gamma}{\langle c_{A\gamma}\rangle^\gamma + K_{A,eq}K_{A\omega}}\frac{\langle c_{B\gamma}\rangle^\gamma}{\langle c_{B\gamma}\rangle^\gamma + K_{B,eq}K_{B\omega}}}_{\text{Reaction}}. \tag{37}$$

Here, $\mathbf{f}_{A\omega}$ and $\mathbf{f}_{A\gamma}$ are the unclosed vectors that define the hydrodynamic dispersive flux as defined above. In this form, the mass balance equation is presented in terms of the fluid-phase concentration, $\langle c_{A\gamma}\rangle^\gamma$, which is generally the concentration that would be measurable in experimental work or in applications to the field.

Although Eqs. (33) and (37) are balance equations for the macroscopic concentration, they are not yet closed forms because each also contains the quantities $\tilde{c}_{A\gamma}$ and $\tilde{c}_{A\omega}$ as independent variables in the area integrals. This is typical of upscaling procedures: one finds that the macroscopic behavior of the system is dependent upon certain integral measures of the microscale physics and structure. In order to close the problem, we must develop a means of expressing the deviation concentrations as a function of only the volume averaged concentrations, $\langle c_{A\gamma}\rangle^\gamma$ and $\langle c_{A\omega}\rangle^\omega$ (or $\{c_A\}$), and the independent parameters that appear in the problem. Closure of the macroscopic transport equation is discussed in detail in the following section.

4. Closure

4.1. Derivation of the closure problem for a periodic unit cell

The development of the macroscale transport equation via averaging, as detailed above, accomplishes two important goals: (1) it establishes the correct mathematical form of the macroscopic transport equation, and (2) it provides constraints that indicate under what conditions the averaged transport equation is valid. These two steps are useful in themselves even without further development; in fact, many averaging techniques posit these to objectives as their terminal goal. However, if one is interested in also understanding how the microscale phenomena and geometric structure influence the macroscale equations, one must also find a method to eliminate explicit involvement of the microscale quantities $\tilde{c}_{A\gamma}$ and $\tilde{c}_{A\omega}$. Eliminating the explicit involvement of such microscale quantities requires hypothesizing some kinds of scaling laws. Scaling laws are axiomatic statements about some element of the structure of the microscale fields involved in the transport problem. Often scaling laws are expressed as indicating that the microscale fields have a particular spatial or temporal statistical structure (e.g., the fields are second-order spatially stationary or spatially periodic); a more extensive discussion of the concepts of scaling laws can be found in the reference by Wood [80]. Note that there is a significant analogy here with the theory of turbulence, where an upscaled momentum balance can be developed, but must be subsequently closed to eliminate an explicit dependence upon microscale velocity fluctuations.

In the present work, in order to close the macroscopic transport equation we must have a means of relating the perturbation concentrations $\tilde{c}_{A\gamma}$ and $\tilde{c}_{A\omega}$ in terms of the volume average concentrations $\langle c_{A\gamma}\rangle^\gamma$ and $\langle c_{A\omega}\rangle^\omega$. One can rearrange the definition of the deviation concentrations given in Eqs. (14) and (15) to the form

$$\tilde{c}_{A\omega} = c_{A\omega} - \langle c_{A\omega}\rangle^{\omega}, \tag{38}$$

$$\tilde{c}_{A\gamma} = c_{A\gamma} - \langle c_{A\gamma}\rangle^{\gamma}. \tag{39}$$

This form suggests that we can develop the governing differential equation for the deviation concentrations by subtracting the averaged equations from the point equations. To determine the conservation equations for the deviation quantities, one can subtract Eq. (16) from Eq. (1) and Eq. (17) from Eq. (6). Under conditions of local mass equilibrium, it can be shown (Appendix B) that the set of equations that predicts the deviation quantities is given by

Closure problem

$$\begin{aligned}\frac{\partial \tilde{c}_{A\omega}}{\partial t} &= \nabla\cdot(\mathbf{D}_{A\omega}\cdot\nabla\tilde{c}_{A\omega}) - \varepsilon_{\omega}^{-1}\nabla\\ &\cdot\left[\varepsilon_{\omega}\mathbf{D}_{A\omega}\cdot\left(\frac{1}{V_{\omega}}\int_{A_{\omega\gamma}(t)}\mathbf{n}_{\omega\gamma}\tilde{c}_{A\omega}\,dA + \frac{1}{V_{\omega}}\int_{A_{\omega\kappa}(t)}\mathbf{n}_{\omega\kappa}\tilde{c}_{A\omega}\,dA\right)\right]\\ &-\frac{1}{V_{\omega}}\int_{A_{\omega\kappa}(t)}\mathbf{n}_{\omega\kappa}\cdot(\mathbf{D}_{A\omega}\cdot\nabla\tilde{c}_{A\omega})dA\\ &-\frac{1}{V_{\omega}}\int_{A_{\omega\gamma}(t)}\mathbf{n}_{\omega\kappa}\cdot(\mathbf{D}_{A\omega}\cdot\nabla\tilde{c}_{A\omega})dA,\end{aligned} \tag{40}$$

B.C.1
$$-\mathbf{n}_{\omega\kappa}\cdot\mathbf{D}_{A\omega}\cdot\nabla\tilde{c}_{A\omega} = \underbrace{\mathbf{n}_{\omega\kappa}\cdot\mathbf{D}_{A\omega}\cdot\nabla\langle c_{A\omega}\rangle^{\omega}}_{\text{dispersive source}} \quad \text{at } A_{\omega\kappa}, \tag{41}$$

B.C.2
$$-\mathbf{n}_{\gamma\kappa}\cdot\mathbf{D}_{A\gamma}\nabla\tilde{c}_{A\gamma} = \underbrace{\mathbf{n}_{\gamma\kappa}\cdot\mathscr{D}_{A\gamma}\nabla\langle c_{A\gamma}\rangle^{\gamma}}_{\text{dispersive source}} \quad \text{at } A_{\gamma\kappa}, \tag{42}$$

B.C.3
$$\tilde{c}_{A\gamma} = K_{A,eq}\tilde{c}_{A\omega} \quad \text{at } A_{\gamma\omega}, \tag{43}$$

B.C.4
$$\begin{aligned}\mathbf{n}_{\gamma\omega}\cdot\mathscr{D}_{A\omega}\cdot\nabla\tilde{c}_{A\omega} &= \mathbf{n}_{\gamma\omega}\cdot\mathscr{D}_{A\gamma}\nabla\tilde{c}_{A\gamma}\\ &+\underbrace{\mathbf{n}_{\gamma\omega}\cdot(\mathscr{D}_{A\gamma}\mathbf{I} - K_{A,eq}^{-1}\mathbf{D}_{A\omega})\cdot\nabla\langle c_{A\gamma}\rangle^{\gamma}}_{\text{dispersive source}}\\ &\text{at } A_{\gamma\omega},\end{aligned} \tag{44}$$

$$\begin{aligned}\frac{\partial\tilde{c}_{A\gamma}}{\partial t} + \tilde{\mathbf{v}}_{\gamma}\cdot\nabla\langle c_{A\gamma}\rangle^{\gamma} + \mathbf{v}_{\gamma}\cdot\nabla\tilde{c}_{A\gamma} &= \nabla\cdot(\mathscr{D}_{A\gamma}\nabla\tilde{c}_{A\gamma}) + \varepsilon_{\gamma}^{-1}\nabla\cdot\langle\tilde{\mathbf{v}}_{\gamma}\tilde{c}_{A\gamma}\rangle\\ &-\varepsilon_{\gamma}^{-1}\nabla\cdot\left[\varepsilon_{\gamma}\mathbf{D}_{A\gamma}\left(\frac{1}{V_{\gamma}}\int_{A_{\omega\gamma}(t)}\mathbf{n}_{\gamma\omega}\tilde{c}_{A\gamma}\,dA\right.\right.\\ &\left.\left.+\frac{1}{V_{\gamma}}\int_{A_{\omega\kappa}(t)}\mathbf{n}_{\gamma\kappa}\tilde{c}_{A\gamma}\,dA\right)\right]\\ &-\frac{1}{V_{\gamma}}\int_{A_{\omega\gamma}(t)}\mathbf{n}_{\gamma\omega}\cdot(\mathscr{D}_{A\gamma}\nabla\tilde{c}_{A\gamma})dA\\ &-\frac{1}{V_{\gamma}}\int_{A_{\omega\kappa}(t)}\mathbf{n}_{\gamma\kappa}\cdot(\mathscr{D}_{A\gamma}\nabla\tilde{c}_{A\gamma})dA.\end{aligned} \tag{45}$$

The solutions to these equations can, in principle, be expressed by time-space convolution integrals of the source terms with the appropriate Greens functions. Under the conditions that have already been imposed in the analysis (cf. Section A.2, Appendix A), the source terms can be removed from the convolutions, and this yields solutions that take the algebraic form (cf. [76,79]; Section B.2)

$$\tilde{c}_{A\omega} = \mathbf{b}_{A\omega}\cdot\nabla\langle c_{A\omega}\rangle^{\omega}, \tag{46}$$

$$\tilde{c}_{A\gamma} = \mathbf{b}_{A\gamma}\cdot\nabla\langle c_{A\gamma}\rangle^{\gamma}. \tag{47}$$

Further discussion of the solution in terms of Greens functions can be found in the recent paper by Wood [80].

Note that in Eq. (33) the deviation concentrations $\tilde{c}_{A\omega}$ and $\tilde{c}_{A\gamma}$ appear only under the integrals associated with Eqs. (34) and (35). Because of this, the dependence of the dispersion tensor upon the solution to the closure problem is weak in the sense that it depends only on integrated quantities [40]. Any local solution for $\tilde{c}_{A\omega}$ and $\tilde{c}_{A\gamma}$ that produces acceptable values of the area integrals can be used to determine the effective dispersion tensor. One reasonable model might be to impose the condition that the deviations are identically zero on the boundaries. For our purposes, a *periodic model* of a heterogeneous porous medium is convenient (and imposes less severe constraints on the problem than, say, a Dirichlet condition would). In terms of the single periodic unit cell, the local closure problem can then be specified in the dimensionless form.

Closure problem (dimensionless form)

$$\begin{aligned}0 &= \nabla\cdot(\mathbf{D}_{\Gamma}\cdot\nabla\mathbf{b}'_{A\omega}) - \frac{1}{V_{\omega}}\int_{A_{\omega\gamma}(t)}\mathbf{n}_{\omega\gamma}\cdot(\mathbf{D}_{\Gamma}\cdot\nabla\mathbf{b}'_{A\omega})dA\\ &-\frac{1}{V_{\omega}}\int_{A_{\omega\kappa}(t)}\mathbf{n}_{\omega\kappa}\cdot(\mathbf{D}_{\Gamma}\cdot\nabla\mathbf{b}'_{A\omega})dA,\end{aligned} \tag{48}$$

B.C.1
$$-\mathbf{n}_{\omega\kappa}\cdot\mathbf{D}_{\Gamma}\cdot\nabla\mathbf{b}'_{A\omega} = \mathbf{n}_{\omega\kappa}\cdot\mathbf{D}_{\Gamma} \quad \text{at } A_{\omega\kappa}, \tag{49}$$

B.C.2
$$-\mathbf{n}_{\gamma\kappa}\cdot\nabla\mathbf{b}'_{A\gamma} = \mathbf{n}_{\gamma\kappa} \quad \text{at } A_{\gamma\kappa}, \tag{50}$$

B.C.3
$$\mathbf{b}'_{A\gamma} = \mathbf{b}'_{A\omega} \quad \text{at } A_{\gamma\omega}, \tag{51}$$

B.C.4
$$\begin{aligned}-\mathbf{n}_{\gamma\omega}\cdot\mathbf{D}_{\Gamma}\cdot\nabla\mathbf{b}'_{A\omega} &= \mathbf{n}_{\gamma\omega}\cdot\nabla\mathbf{b}'_{A\gamma}\\ &+\underbrace{\mathbf{n}_{\gamma\omega}\cdot(\mathbf{I}-\mathbf{D}_{\Gamma})}_{\text{dispersive source}} \quad \text{at } A_{\omega\kappa},\end{aligned} \tag{52}$$

$$\begin{aligned}Pe_A(\tilde{\mathbf{v}}'_{\gamma} + \mathbf{v}'_{\gamma}\cdot\nabla\mathbf{b}'_{A\gamma}) &= \nabla^2\mathbf{b}'_{A\gamma} - \frac{1}{V_{\gamma}}\int_{A_{\omega\gamma}(t)}\mathbf{n}_{\gamma\omega}\cdot\nabla\mathbf{b}'_{A\gamma}dA\\ &-\frac{1}{V_{\gamma}}\int_{A_{\omega\kappa}(t)}\mathbf{n}_{\gamma\kappa}\cdot\nabla\mathbf{b}'_{A\gamma}dA,\end{aligned} \tag{53}$$

B.C.5 (Periodicity)
$$\mathbf{b}'_{A\omega}(\mathbf{r}) = \mathbf{b}'_{A\omega}(\mathbf{r}+\ell_i), \quad i=1,2,3, \text{ at } A_{\omega e}, \tag{54}$$

B.C.6 (Periodicity)
$$\mathbf{b}'_{A\gamma}(\mathbf{r}) = \mathbf{b}'_{A\gamma}(\mathbf{r}+\ell_i), \quad i=1,2,3, \text{ at } A_{\gamma e}, \tag{55}$$

B.C.7
$$\langle\mathbf{b}'_{A\gamma}\rangle^{\gamma} = 0, \tag{56}$$

B.C.8
$$\langle\mathbf{b}'_{A\omega}\rangle^{\omega} = 0, \tag{57}$$

where $A_{\omega e}$ and $A_{\gamma e}$ represent the areas of the entrances and exits of the ω- and γ-phases at the boundaries of the unit cell. In these expressions, the following dimensionless variables and parameters have been defined by

$$\mathbf{b}'_{A\gamma} = \frac{\mathbf{b}_{A\gamma}}{\ell_{\gamma}}; \quad \mathbf{b}'_{A\omega} = \frac{\mathbf{b}_{A\omega}}{\ell_{\gamma}}, \tag{58}$$

$$\tilde{\mathbf{v}}'_{\gamma} = \frac{\tilde{\mathbf{v}}_{\gamma}}{\|v_{\gamma}\|}; \quad \mathbf{v}'_{\gamma} = \frac{\mathbf{v}_{\gamma}}{\|v_{\gamma}\|}, \tag{59}$$

$$\mathbf{D}_{\Gamma} = \frac{K_{A,eq}^{-1}\mathbf{D}_{A\omega}}{\mathscr{D}_{A\gamma}}. \tag{60}$$

The use of a spatially periodic model for closure is often misinterpreted, and some additional comments about this closure scheme are warranted. The use of spatially periodic model does not imply that the results apply only to periodic media or that the structure of the porous medium is actually assumed to be periodic (see the

discussions by Chrysikopoulos et al. [9], Eames and Bush [16], Pickup et al. [43], Renard and de Marsily [51] and Wang and Kitanidis [68]). The periodic boundary condition is only a device for obtaining a local solution and it is not necessarily any less suitable than the use of the boundary conditions specified at infinity that are often employed in ensemble averaging methods. A study of the interplay between the unit cell length and the spatial correlation length in the case of randomly generated heterogeneous porous media can be found in Ahmadi and Quintard [1].

4.2. The closed form of the macroscopic transport equation

In the closure problem given by Eqs. (48)–(55), only two dimensionless parameters arise, $\mathbf{D}_\Gamma$ and Pe_A, that have an influence on the calculation of the effective diffusivity for a given unit cell geometry. Note that the Damköhler number does not appear here. The reason for this is that the assumption of local mass equilibrium requires one to neglect the effect of the reaction term in the biofilm phase on the macroscopic dispersion phenomenon. If we use the representations given by Eqs. (46) and (47) we can write the macroscale transport equation in its final closed form as follows:

Macroscopic scale transport equation, fluid-phase concentration form (closed)

$$\begin{aligned}\frac{\partial}{\partial t}(\varepsilon_\gamma + K_{A,eq}^{-1}\varepsilon_\omega)\langle c_{A\gamma}\rangle^\gamma = & -\nabla\cdot(\varepsilon_\gamma\langle\mathbf{v}_\gamma\rangle^\gamma\langle c_{A\gamma}\rangle^\gamma)\\ & +\nabla\cdot(\mathbf{D}^*_{A,eff}\cdot\nabla\langle c_{A\gamma}\rangle^\gamma)\\ & -\varepsilon_\omega\mu_{A\omega}\rho_\omega\frac{\langle c_{A\gamma}\rangle^\gamma}{\langle c_{A\gamma}\rangle^\gamma + K_{A,eq}K_{A\omega}}\\ & \times\frac{\langle c_{B\gamma}\rangle^\gamma}{\langle c_{B\gamma}\rangle^\gamma + K_{B,eq}K_{B\omega}}.\end{aligned}\tag{61}$$

Here, the effective dispersion tensor for the species A, $\mathbf{D}^*_{A,eff}$, is given by

$$\begin{aligned}\mathbf{D}^*_{A,eff} = & (\varepsilon_\gamma\mathscr{D}_{A\gamma}\mathbf{I} + K_{A,eq}^{-1}\varepsilon_\omega\mathbf{D}_{A\omega})\\ & +\mathscr{D}_{A\gamma}\left(\frac{1}{\mathscr{V}}\int_{A_{\omega\gamma}(t)}\mathbf{n}_{\gamma\omega}\mathbf{b}_{A\gamma}\,dA+\frac{1}{\mathscr{V}}\int_{A_{\gamma\kappa}(t)}\mathbf{n}_{\gamma\kappa}\mathbf{b}_{A\gamma}\,dA\right)\\ & +K_{A,eq}^{-1}\mathbf{D}_{A\omega}\cdot\left(\frac{1}{\mathscr{V}}\int_{A_{\omega\gamma}(t)}\mathbf{n}_{\omega\gamma}\mathbf{b}_{A\omega}dA+\frac{1}{\mathscr{V}}\int_{A_{\omega\kappa}(t)}\mathbf{n}_{\omega\kappa}\mathbf{b}_{A\omega}dA\right)\\ & -\langle\tilde{\mathbf{v}}_\gamma\mathbf{b}_{A\gamma}\rangle.\end{aligned}\tag{62}$$

Eq. (62) begins to make it more apparent how the microscale and macroscale properties are related. Each of the area integrals shown above represents quantities that influence the effective diffusion coefficient of the porous media and biofilm system; such representations have been known for literally over one hundred years [31,50]. It has been established in numerous studies that, for spatially isotropic media, the effective diffusion coefficient is a function of primarily the volume fraction of the fluid (or, in this case, the fluid and biofilm) phases [45]. The final term on the right-hand side of Eq. (62) represents a volume average of the fluctuations of the velocity field, and this quantity is associated with hydrodynamic dispersion.

The quantities that would have to be measured, or otherwise estimated, in order to solve the closure problem for a representative unit cell are as follows: (1) the effective diffusion coefficient for the biofilm, (2) the diffusion coefficient for the free fluid, (3) the partitioning coefficient, $K_{A,eq}$, if it is different from unity, (4) the geometric structure of the fluid, solid, and biofilm phases within the unit cell, and (5) the velocity field within the fluid phase. The effective diffusion coefficient in biofilms can be either measured experimentally (e.g. [60]) or estimated from previous theoretical developments (e.g. [75]); the diffusion coefficient for free fluid has been tabulated in the literature for a wide variety of dilute solutes. The partitioning coefficient is taken to be unity for many solutes, but for some (in particular, hydrophobic solutes) a partitioning coefficient less than unity has been measured [36]. Finally, in principle both the geometric structure and flow field are measurable at the microscale using a variety of experimental methods (e.g., magnetic resonance imaging, as described by Seymour et al. [55]). However, as discussed below, it may also be possible to use a representative unit cell that is abstracted from the complexities of a fully three-dimensional complex unit cell that maps biofilm, fluid, and solids separately at high resolution. The reason that such abstractions can be useful is that in many instances (e.g., the case of diffusion in isotropic porous media) the actual physical geometry of the system is of secondary importance compared with, for example, achieving the correct volume fraction for each of the phases present. The issue of simplifications to the unit cell will be explored further in the material that follows.

5. Results and discussion

In the closed form of the transport equation given by Eq. (61), the expression of the effective parameter $\mathbf{D}^*_{A,eff}$ requires the knowledge of the closure variables $\mathbf{b}_{A\gamma}$ and $\mathbf{b}_{A\omega}$, and this requires that the differential equations describing the closure problem [Eqs. (48)–(55)] be solved. In this section, we describe the solution to the closure problem and the calculation for the effective dispersion tensor for two kinds of unit cells: (1) simple, and (2) complex.

5.1. Simple unit cells

As discussed above, the effective dispersion tensor depends on integrals of the $\mathbf{b}_{A\gamma}$ and $\mathbf{b}_{A\omega}$ fields that are defined by the closure problem. In the solution of closure problems, geometries that are substantially abstracted from the complexities of the real system often still contain enough of the important physical features such that they produce very accurate results. The most famous examples of this is Maxwell's [31] and Rayleigh's [50] solutions for the effective conductivity of a two-material conductor; this same result is used extensively in describing the effective diffusion coefficient for multiphase systems (e.g. [22,75,78]).

It has been previously recognized (e.g. [79]) that 'simple' unit cells tend to underestimate the magnitude of the effective dispersion tensor because they do not contain important particle–particle correlation in the unit cell structure. However, there is essentially no *a priori* method to determine how much geometric structure is sufficient to adequately represent the transport processes within a unit cell. Part of the problem is that the structure necessary depends upon the form of the mathematical operators involved. To address this issue, different types of unit cells, represented in Fig. 3 and denoted from (a) to (d) were examined as detailed below. Most important features which characterise unit cells are gathered in Table 1. The volume fraction of the κ-phase is kept constant in all configurations and fixed at 0.3. We assume also that there is no concentration jump between the fluid and biofilm phases, i.e., $K_{A,eq} = 1$.

The comparison of results obtained on these geometries has led to a better understanding of the impact of the different characteristic features on which the dispersion tensor depends – in particular its dependence on, (1) the diffusion coefficient value, (2) the biofilm volume fraction, (3) the geometry and, (4) the dimensional configuration (2D versus 3D).

The closure problem under consideration in this work is mathematically similar to this one detailed by Wood et al. [78] for transport within a porous medium containing biofilm. Thus, we follow essentially the same procedure here.

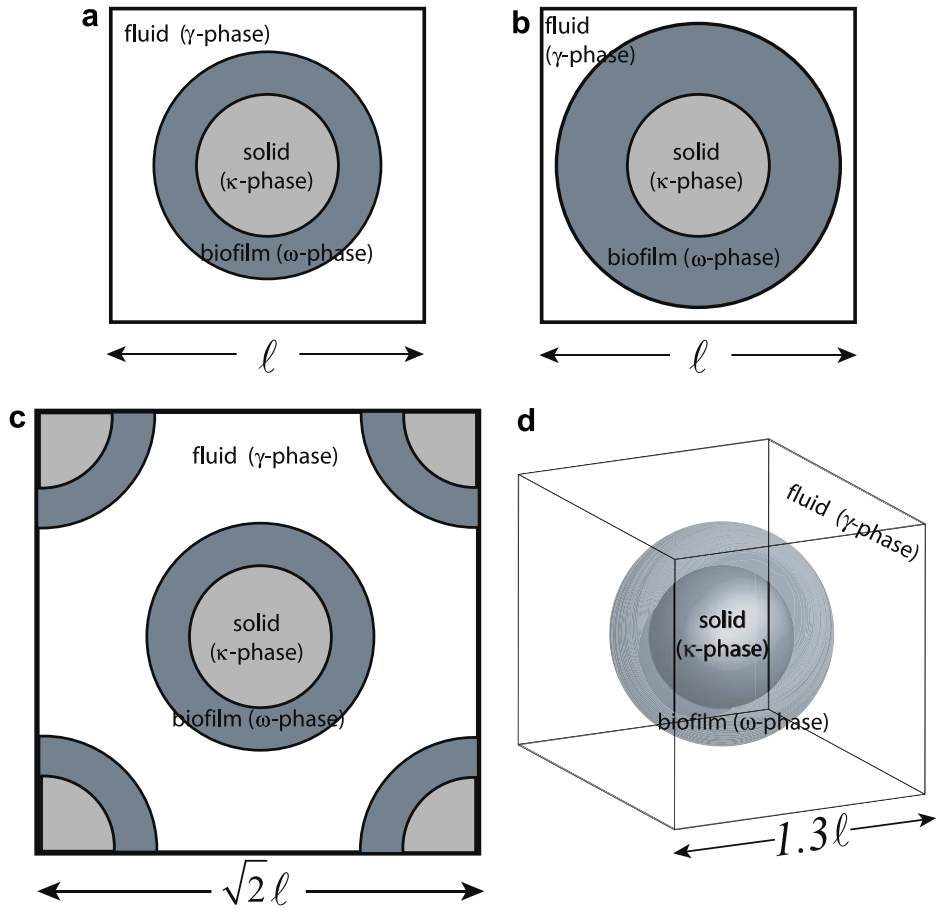

Fig. 3. Unit cells used for making computations.

Table 1
The physical parameters associated with various unit cells.

Parameter	Unit cell			
	(a)	(b)	(c)	(d)
Diffusion volume fraction ($\varepsilon_\omega + \varepsilon_\gamma$)	0.70	0.70	0.70	0.70
Biofilm volume fraction ε_ω	0.10	0.45	0.10	0.10
Packing configuration	In-line	In-line	Staggered	In-line
Dimensional configuration	2D	2D	2D	3D

The adopted numerical model is based on a finite volume formulation. The porous medium geometry is described by assigning fluid, biofilm or solid properties to the block of Cartesian grid. A grid of 250 × 250 nodes (200 × 200 × 200 in 3D) is used and provides sufficient resolution for obtaining accurate results. A convergence analysis has confirmed independence of the results on grid resolution. The first step consists of computing the velocity field over the given unit cell. The discretisation of the Stokes equations does not pose major problems and a classical Uzawa algorithm [19] is adopted for computing the pressure. The convective transport terms are discretised using an upstream scheme and numerical dispersion is limited by locally correcting the diffusion terms [49]. Finally, the resulting linear system is solved with the algorithm BI-CGSTAB [66].

Numerical computations performed further for these different configurations are given in terms of the cell Péclet number, defined by Eq. (28), for values varying between 0.001 and 1000. The characteristic length ℓ_γ which appears in this expression is taken equal to the unit cell length ℓ, as illustrated in Fig. 3. As a comparison note that, for bioreactors, Péclet numbers vary typically between 0.1 and 10. All computations are made for an averaged velocity field in the *x*-direction. Thus, the *xx*-component of the dispersion tensor corresponds to longitudinal dispersion.

5.1.1. Impact of the diffusion ratio $\mathscr{D}_\Gamma$: comparison between active and passive dispersion – configuration (a)

We examined unit cell (a) for two distinct values of the diffusion ratio, $\mathscr{D}_\Gamma = 0.001$ and $\mathscr{D}_\Gamma = 1$. In Fig. 4 this comparison is shown for the longitudinal dispersion. For the first case $\mathscr{D}_\Gamma \to 0$ (i.e., the diffusion in biofilm phase is negligible), the problem reduces to the case of pure passive dispersion (cf. [70; Eq. (3.3.40)]). The second simulation corresponds to the other limit case where the diffusion coefficient in both phases is equal. By passive dispersion we mean that there is no adsorption or reaction at $A_{\gamma\omega}$ interface, and there is no transport from the γ-phase into the ω-phase (cf. [46]). When there is multiphase transport and/or reactions, the literature has adopted the terminology 'active dispersion'.

These results feature the classical distinct regimes for the flow rate dependency of the effective dispersion tensor. At low Péclet number (regime I represented in Fig. 4), solute dispersion is only driven by diffusion phenomena. Note that in this regime the influence of biofilm activity is clearly pointed out. The biofilm phase which is usually a region of lower diffusion, reduces dispersion within the domain. When the Péclet number increases, a transition regime (regime II) appears where both diffusion and convection processes affect the dispersion. Finally, at high Péclet numbers (regime III), dispersion phenomena predominate over solute transport and $D^*_{A,xx}$ (where $D^*_{A,xx}$ is the notation that we have adopted for the

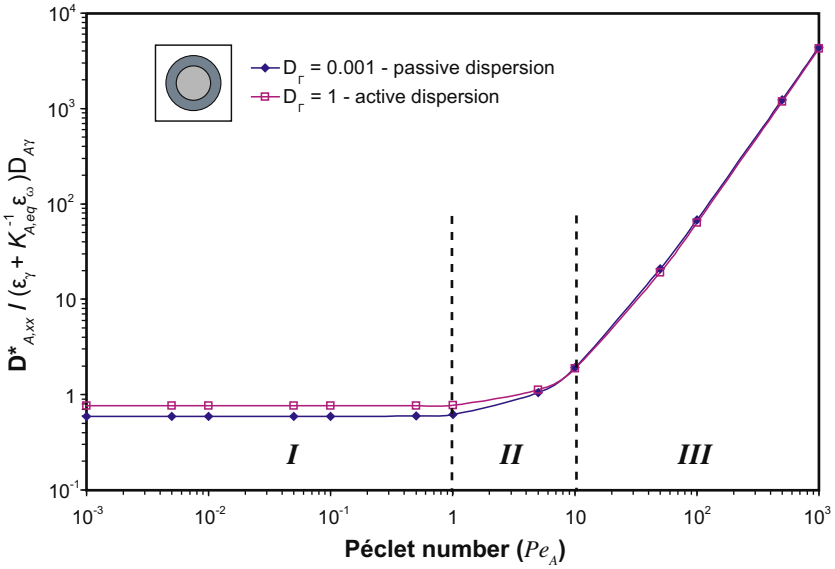

Fig. 4. Comparison between active and passive dispersion – unit cell (a), $\varepsilon_\omega = 0.10$.

xx-component of the dispersion tensor $\mathbf{D}^*_{A.eff}$) becomes exponentially dependent on Péclet number. The power-law exponent, denoted by δ, expressing this Péclet number dependence, varies as a function of geometry as we will see later and is close to 1.8 here. Both curves converge practically to the same asymptotic value. Diffusion in the biofilm phase contributes to the slight reduction of the effective dispersion coefficient observed.

5.1.2. Impact of the biofilm volume fraction – configuration (a) and (b)

An example of typical results for the *xx*-component of the dispersion tensor obtained for two different volume fractions of biofilm (configuration a and b) is illustrated in Fig. 5. The diffusion ratio, $\mathscr{D}_\Gamma$, is fixed at 0.5. It is clear from this figure that the biofilm development significantly influences the dispersion phenomena at low Péclet number values as well as at high ones. The more biofilm volume fraction increases, the more the dispersion tensor component decreases compared to the one predicted for the case of no biofilm ($\varepsilon_\omega = 0$). As the biofilm grows, the volume fraction of the biofilm ε_ω increases; because the diffusion coefficient in the biofilm is smaller than it is for the free fluid, this impacts the diffusive portion of the dispersion tensor. Because of growth the volume fraction of the fluid-phase, ε_γ, contributing to the convection, decreases; the result of this is that the mechanical component of the dispersion coefficient is also decreased.

5.1.3. Impact of the geometry – configuration (a) and (c)

The results reported in Fig. 6 illustrate the impact of geometry on the longitudinal and transverse dispersion coefficients. Two types of structure, in-line (unit cell a) and staggered (unit cell c), are tested here. For these simulations, the diffusion ratio, $\mathscr{D}_\Gamma$, remains equal to 0.5.

At low Péclet numbers ($Pe_A < 1$), the same value of the effective diffusion is obtained for both geometries. This confirms that the effective diffusion coefficient is essentially determined by the volume fractions of the three phases (cf. [45]). When Péclet number increases ($Pe_A > 1$), convection becomes dominant in the dispersion

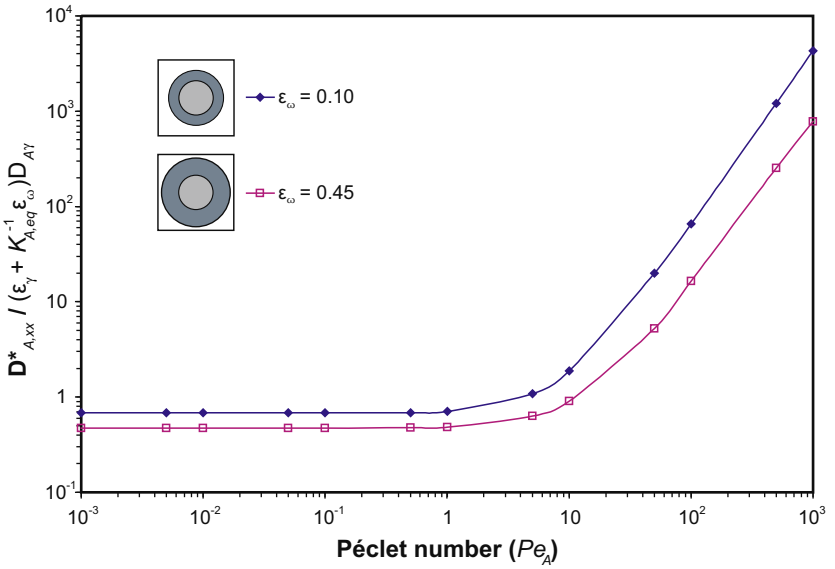

Fig. 5. Influence of the biofilm volume fraction. Results for unit cell (b) and (c) are shown with $\mathscr{D}_\Gamma = 0.5$.

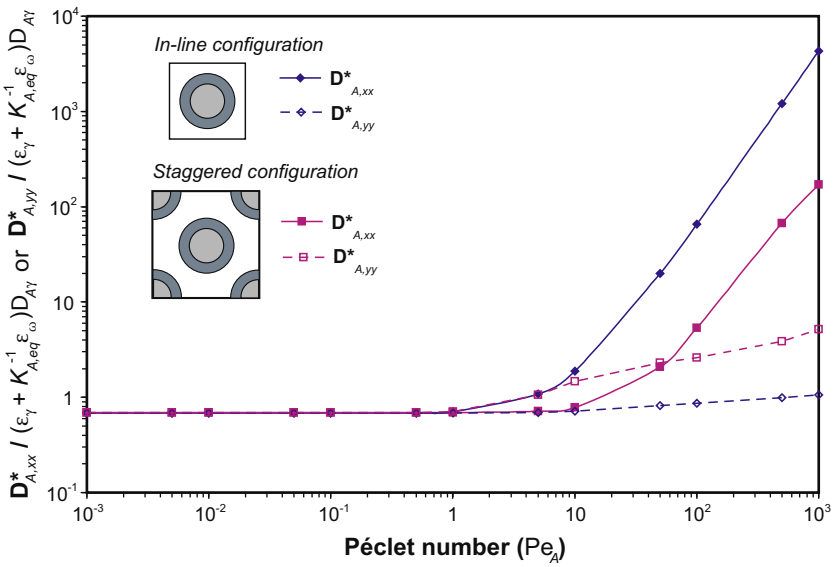

Fig. 6. Influence of the geometry of the unit cell. Results for unit cell (a) and (c) are shown with $\mathscr{D}_\Gamma = 0.5$.

process, and this causes the two different geometries to exhibit different behavior for the mechanical component of the dispersion tensor. For a Péclet number of 1000, for instance, the values of $D^*_{A,xx}$ for in-line systems would be more than one order of magnitude larger than the values of $D^*_{A,xx}$ for more complex systems. Similar results were obtained for passive dispersion [46] and active dispersion during migration of a NAPL pollutant [48], and it is also consistent with the differences observed in a staggered and square arrays by Knutson et al. [28].

The mass transfer process for an in-line arrangement of cylinders is quite similar to the Taylor dispersion in a capillary tube, which has a Péclet number dependence of the form

$$D^*_{A,xx} \propto Pe^{\delta}, \tag{63}$$

where $\delta = 2$ for the Taylor dispersion case [62,3]. From our numerical results, the Péclet number dependence obtained for the two-dimensional unit cell (a) yields and exponent of $\delta = 1.8$. For a staggered two-dimensional unit cell arrangement, the exponent is $\delta = 1.5$. This change of the Péclet number dependence is due to the change in geometry structure of the periodic array. Note that δ decreases when ε_ω increases for the staggered geometry; e.g. $\delta = 1.2$ for $\varepsilon_\omega = 0.3$. As a comparison, this dependence is less pronounced for the square geometry; e.g., for the unit cell (b) with $\varepsilon_\omega = 0.45$, we obtain $\delta = 1.67$.

As the dispersion effects for the square packing are essentially oriented in the flow direction, i.e., longitudinal, the substrate dispersion along the transverse direction is driven primarily by molecular diffusion and does not vary significantly as a function of the Péclet number. Unit cell (c) shows a more significant dependence upon the Péclet number. At $Pe_A = 10^3$, for instance, a ratio of $D^*_{A,xx}/D^*_{A,yy} = 10$ is observed instead of the ratio $D^*_{A,xx}/D^*_{A,yy} = 10^4$ for the in-line configuration. The transverse dispersion is dramatically enhanced by the staggered arrangement due to the nature more complex of the flow, which begins to approach the structure of a random arrangement (which is explored in more detail below).

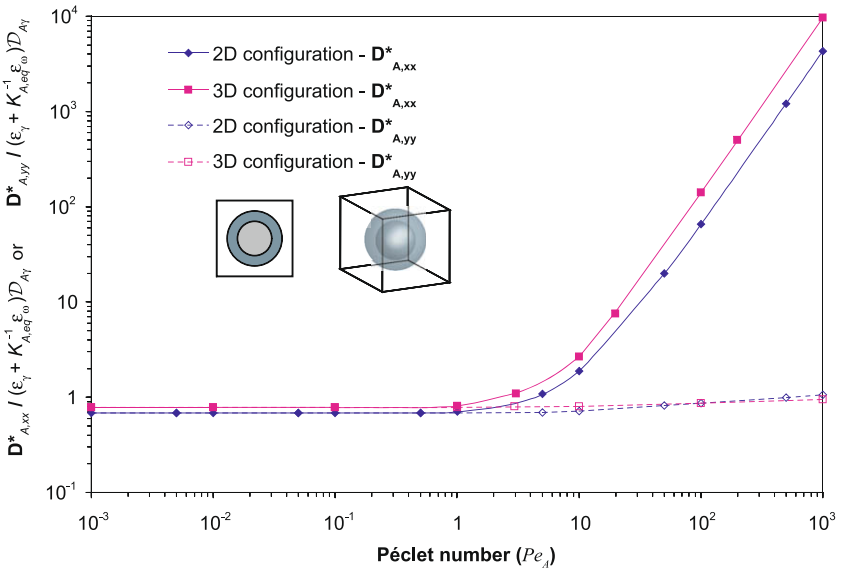

Fig. 7. Comparison between 2D and 3D configurations. Results for unit cell (a) and (d) are shown with $\mathscr{D}_\Gamma = 0.5$.

5.1.4. Impact of the dimensional configuration – configuration (a) and (d)

In Fig. 7, we have illustrated the comparison between the longitudinal dispersion coefficients developed from two-dimensional and three-dimensional unit cells, respectively (as represented by unit cell (a) and (d)). Both unit cells have equal volume fractions, and $\mathscr{D}_\Gamma$ is fixed at 0.5.

The qualitative behaviour of the dispersion tensor is roughly similar for the two configurations. Thus, Péclet number dependence obtained for the three-dimensional unit cell (d) is similar to this observed for two-dimensional case, i.e., $\delta = 1.8$. At low Péclet numbers, although volume fractions are equivalent, one does not recover exactly the same dispersion coefficient due to differences of biofilm thickness. This small discrepancy is amplified with increasing Péclet numbers for the longitudinal dispersion coefficient. The reason for this is that two-dimensional systems generate a more intense lateral convection than does the corresponding three-dimensional system. Similar trends have been obtained for active dispersion of NAPL [2].

The results thus far can be summarized as follows:

1. At low Péclet numbers, dispersion coefficient is essentially determined by volume fractions of the system.
2. The geometry of the system (e.g., staggered versus in-line configurations) influences both the magnitude and the rate of increase (as measured by the power-law exponent, δ) of the dispersion tensor components. The increase of biofilm volume fraction contributes to reduce the dispersion at both low and high Péclet numbers.
3. The qualitative behavior between 2D and 3D unit cells is similar, although the value of the longitudinal dispersion can be different in magnitude.

5.2. Complex unit cells

Although simple unit cells can be a useful abstraction, it is ultimately best to compare with the results that would be predicted by more realistically structured unit cells. It is known from many previous studies on pure passive dispersion that simple unit cells lead to a quantitative behavior that is different from more complex disordered unit cells once one has a significant mechanical component to dispersion. In this section, we examine the solution to the closure problem in unit cells whose structure is taken from magnetic resonance microscopy (MRM) used to generate tomographic mappings of a porous medium at micron-scale resolution. In Fig. 8a, we have shown a small (7.5 mm diameter, 8 mm packed length) column of nominally 250 μm polystyrene beads under saturated conditions. This bead pack was imaged using T2-weighted MRM methods at 30 μm isotropic resolution [30]. Although in principle it may be ultimately possible to simultaneously image the solid, fluid, and biofilm phases at a high isotropic resolution using MRM, this is currently an area of active research (e.g. [56]). Therefore, we have adopted the following strategy to generate a reasonable distribution of biofilm within the measured porous medium structure. First, we numerically increased the resolution of the porous medium map to an isotropic 4 μm and generated a reasonable representation of the biofilm phase by using a cellular automaton model [41]. We obtained the medium structure illustrated in Fig. 8b whose volume fractions are $\varepsilon_\kappa = 0.57$, $\varepsilon_\gamma = 0.31$ and $\varepsilon_\omega = 0.12$. An appropriate characteristic length ℓ_γ for use with the Péclet number is the integral scale, I_{xx}

$$I_{xx} = \int_{\lambda=0}^{\lambda=\infty} C_{xx}(x, x+\lambda)d\lambda. \tag{64}$$

Here C_{xx} is the (assumed spatially stationary) covariance function for the indicator function for the γ-phase, $\psi_\gamma(\mathbf{x})$, defined by

$$\psi_\gamma(\mathbf{x}) = \begin{cases} 1 & \text{for } \mathbf{x} \text{ located in the } \gamma\text{-phase,} \\ 0 & \text{otherwise.} \end{cases} \tag{65}$$

Longitudinal and transverse components of the dispersion tensor calculated on such geometry are presented in Fig. 9. Results are compared with those obtained on a three-dimensional staggered unit cell (similar to configuration (c) but in 3D) equivalent in terms of volume fraction. Note that for this ordered unit cell, the two transverse components are identical.

Several interesting remarks can be extracted from closure problems solved in this complex unit cell. First of all, at low Péclet numbers, predicted values of the dispersion tensor components for the simple and the complex unit cells (with equal volume fractions) are not identical. This suggests that it is not only the volume fractions of each phase, but also the interface shape between biofilm and fluid-phases, or at least, the local biofilm thickness, that is required to predict with accuracy the effective diffusivity. Moreover, when the Péclet number increases, the discrepancy between the longitudinal and transverse components of the dispersion tensor is more pronounced for the simplified unit cell. This confirms the observations made in Section 5.1.3. A more complex disordered unit cell leads to results less sensitive to the pore-scale geometry [59], and hence, to the velocity orientation. As a consequence, simple macroscale parameters such as the volume fraction of the phases and associated correlation lengths are not sufficient to cor-

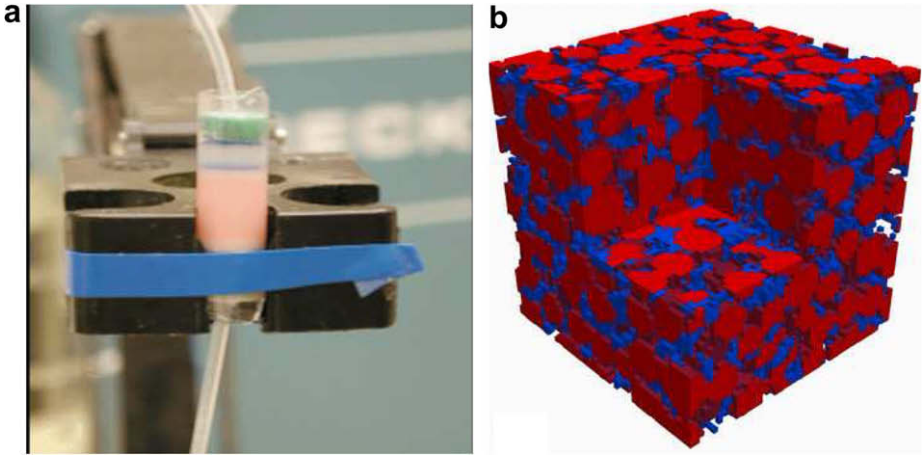

Fig. 8. (a) Experimental column with a 250 μm diameter bead pack containing *S. onidensis* – (b) Unit cell constructed from MRI measurements. Isosurfaces for the solid (red) and biofilm (blue) phases are illustrated. (For interpretation of the references in colour in this figure legend, the reader is referred to the web version of this article.)

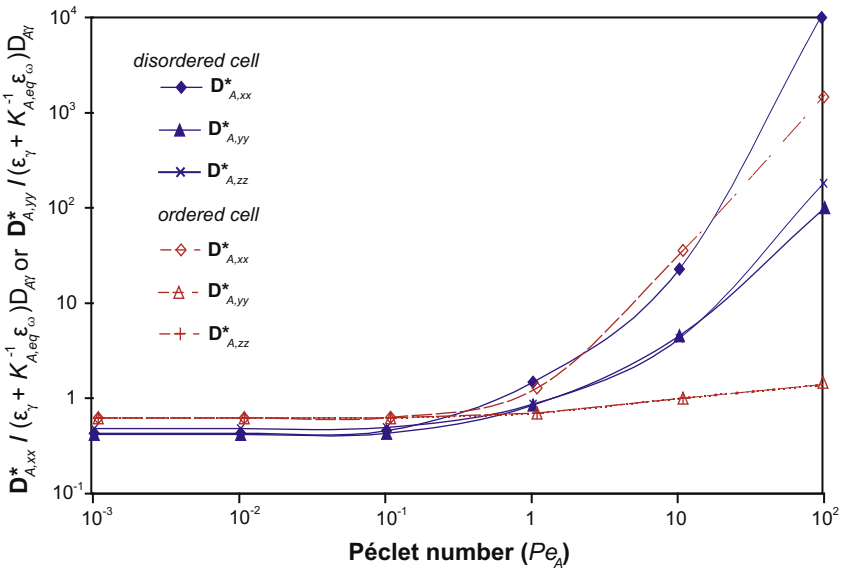

Fig. 9. Comparison of results between the realistically structured and the simplified 3D unit cells.

rectly describe the dispersion phenomenon at high Péclet numbers. In other words, for a particular porous medium, it may be required that one characterizes fully a fairly large representative volume of the porous medium if one wants to predict the dispersion tensor with accuracy.

6. Validity of the upscaled model

6.1. Comparison with direct numerical simulation (DNS)

In this section, we compare results from the one-equation local equilibrium model with those from direct simulations for transient substrate transport in a three-phase system (solid, fluid, and biofilm). In order to test the theoretical development leading to the macroscopic equations and determine the domain of validity of the local mass equilibrium assumption, numerical experiments have been performed on nodular systems. Different types of systems have been used by varying volume fractions. A typical example of such a medium, corresponding to 10 in-line unit cells of dimension $\ell \times \ell$ each, is illustrated in Fig. 10. At the microscale, the physical process will be two-dimensional and transient whereas at the macroscale (associated with the one-equation model), it will be transient and one-dimensional. Eqs. (1)–(6) describe the process at the local-scale in addition to the boundary conditions given below

$$\text{B.C.5} \quad c_{A\gamma} = c_0 \quad \text{at } x = 0, \tag{66}$$

$$\text{B.C.6} \quad \mathbf{n}_y \cdot (\mathscr{D}_{A\gamma} \nabla c_{A\gamma} + \mathbf{v}_\gamma c_{A\gamma}) = 0 \quad \text{at } y = 0, \ell, \tag{67}$$

$$\text{B.C.7} \quad \mathbf{n}_x \cdot \mathscr{D}_{A\gamma} \nabla c_{A\gamma} = 0 \quad \text{at } x = L, \tag{68}$$

$$\text{I.C.} \quad c_{A\omega} = c_{A\gamma} = 0 \quad \text{at } t = 0. \tag{69}$$

Note that the velocity field $\mathbf{v}_\gamma$, considered to be a known field, is found by solving the Stokes equations numerically for the geometry under consideration. In order to simplify the complexity of the problem, we have assumed that the problem is not limited by mass transfer of chemical species *B*. As a consequence, we will have $c_{B\gamma} = c_{B\omega} = 1$ everywhere and $K_{B\omega} \ll c_{B\omega}$. Thus, the dimensionless form of the set of equations for the fluid/biofilm system, Eqs. (1) and (6), reduces to

$$\frac{\partial c'_{A\omega}}{\partial t'} = \nabla \cdot (\mathbf{D}_\Gamma \cdot \nabla c'_{A\omega}) - Da_A \frac{c'_{A\omega}}{1 + \frac{c'_{A\omega}}{K'_{A\omega}}} \quad \text{in the } \omega\text{-phase}, \tag{70}$$

$$\frac{\partial c'_{A\gamma}}{\partial t'} + Pe_A \mathbf{v}'_\gamma \cdot \nabla c'_{A\gamma} = \nabla^2 c'_{A\gamma} \quad \text{in the } \gamma\text{-phase}, \tag{71}$$

where

$$c'_{A\omega} = \frac{c_{A\omega}}{c_0}; \quad c'_{A\gamma} = \frac{c_{A\gamma}}{c_0}; \quad K'_{A\omega} = \frac{K_{A\omega}}{c_0}; \quad t' = \frac{t\mathscr{D}_{A\gamma}}{\ell^2}. \tag{72}$$

We have also assumed that there is no jump in species A concentration between the fluid and biofilm phases (i.e., $K_{eq} = 1$). The dimensionless velocity field that appears in Eq. (71) is obtained by directly solving the Stokes equations within the porous network. From a hydrodynamic point of view, the biofilm phase is treated as a solid where we have imposed a no slip boundary condition at the fluid–biofilm interface; the influence of fluid shear on the biofilm structure is not considered. This appears to be valid for low Reynolds numbers. However, the mechanical interaction between the biofilm and fluid is an area that should be investigated in future work. Convergence analyses (not reported here) were conducted for these simulations to assure that the numerical representation of the transport phenomena were appropriately resolved. The conver-

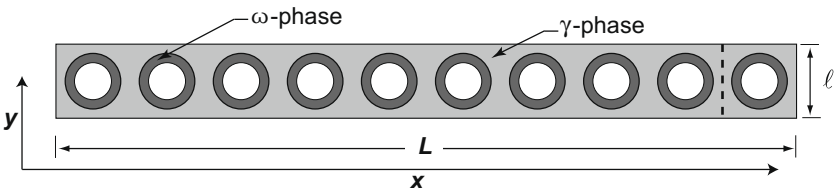

Fig. 10. Illustration of the geometry of the nodular system adopted for direct numerical simulations ($\varepsilon_\kappa = 0.28 - \varepsilon_\omega = 0.22 - \varepsilon_\gamma = 0.5$).

gence analyses suggested that mesh refinement close to the fluid–biofilm interface was required to correctly capture concentration gradients.

Under the limitations of the analysis above, the Péclet and Damköhler numbers are the only leading parameters controlling the substrate transport and consumption within the system. All the simulations presented below will be given in terms of both parameters. From these 'numerical experiments', exact values of volume averaged concentrations of species under consideration can be extracted and compared with those predicted by the theory. As we expect to find differences between theory and numerical experiments near the zone with strong gradients, i.e., $x = 0$, we will compare the transient elution curves at the outlet obtained from the concentration field averaged on the last unit cell on the basis of the *equilibrium-weighted average concentration*. In parallel, calculation of the effective dispersion coefficient has been performed on a representative unit cell for the Péclet and Damköhler values of interest and introduced in the one-equation local equilibrium model.

6.2. Validity of the one-equation model

Both the microscale (DNS) and upscaled sets of equations were solved using the commercial finite-element code COMSOL Multiphysics 3.3, and the results of these simulations were compared. The result of this comparison is represented in Figs. 11–13 for three typical numerical conditions, respectively, $Pe_A = 10^{-1} - Da_A = 10^{-2}$, $Pe_A = 10 - Da_A = 10$, and $Pe_A = 50 - Da_A = 10^{-1}$; $\mathscr{D}_\Gamma$ has been arbitrarily fixed at 0.25 and $K'_{A\omega}$ fixed at 0.5. A number of such direct comparisons were performed; only three of the most informative results are presented here. These results suggest that the local mass equilibrium model is valid for the conditions $Pe_A < 1$ and $Da_A < 1$. If the one-equation model is not valid, then non-equilibrium conditions apply, and a more complex analysis will ultimately be required. A diagram presenting the relationship among the possible regimes (including the results from the simulations performed) is presented in Fig. 14.

We could expect such a result from the observation of constraints given by Eqs. (31) and (32). Indeed, these relationships may be rewritten in the form

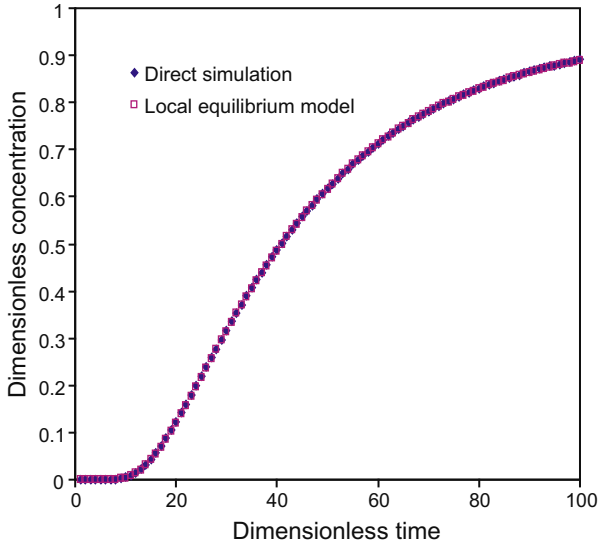

Fig. 11. Comparison between direct numerical simulation and the local equilibrium model with $Pe_A = 10^{-1} - Da_A = 10^{-2}$.

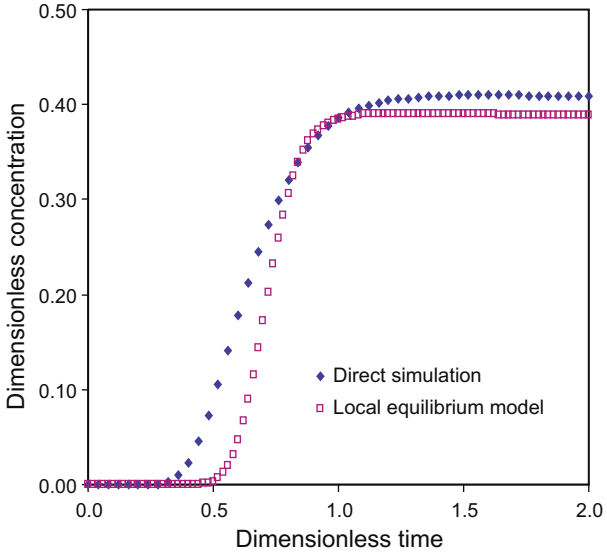

Fig. 12. Comparison between direct numerical simulation and the local equilibrium model with $Pe_A = 10 - Da_A = 10$.

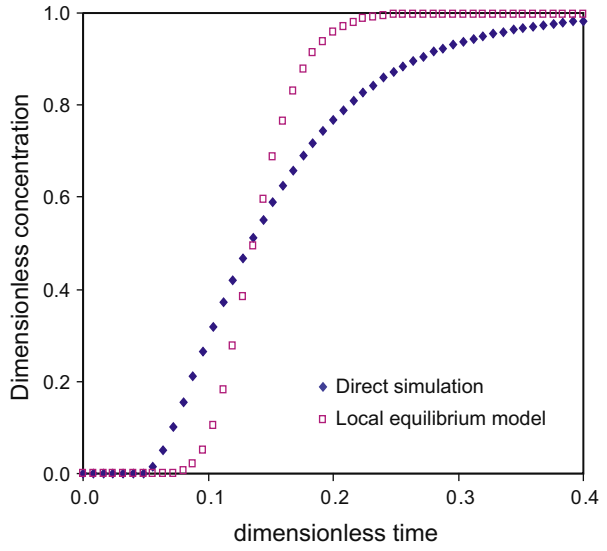

Fig. 13. Comparison between direct numerical simulation and the local equilibrium model with $Pe_A = 50 - Da_A = 10^{-1}$.

$$\mathbf{O}\{Da_A\} \ll 1, \tag{73}$$

$$\mathbf{O}\{Pe_A\} \ll 1. \tag{74}$$

Note that for $Pe_A > 1$ but $Da_A < 1$, even if local equilibrium conditions are not met, the one-equation model captures the correct behavior for the zeroth and first moment of the elution curve; however, the second moment (which is related to the effective dispersion tensor) does not match. For such cases, the one-equation model may still be suitable for applications, depending upon the accuracy required by the user.

7. Conclusions

In this study, we have presented the equations describing the reactive transport in a porous medium at the Darcy-scale within a local equilibrium one-equation model. The constraints associated with the local equilibrium condition and the closure problem directing the effective properties have also been developed. We

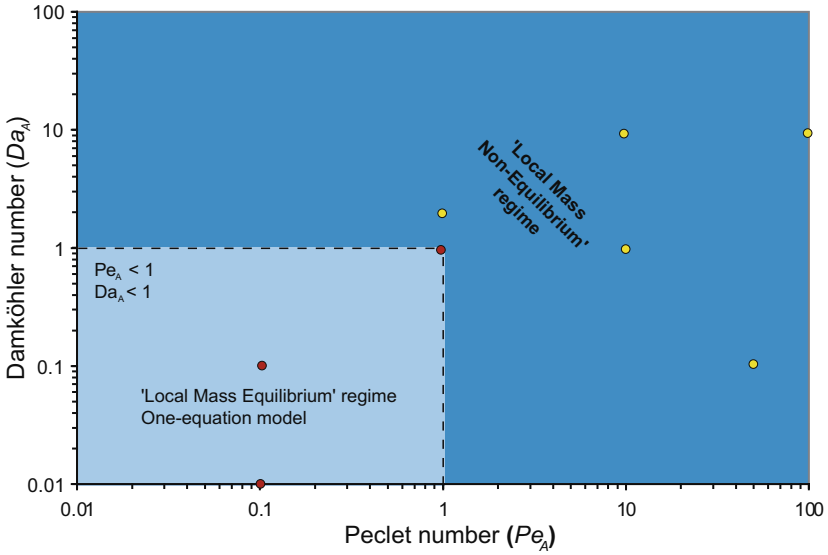

Fig. 14. The domain of validity of the local mass equilibrium regime (red dots – microscale simulations under conditions of local mass equilibrium; yellow dots – microscale simulations corresponding to local mass non-equilibrium conditions). (For interpretation of the references in colour in this figure legend, the reader is referred to the web version of this article.)

could thus evaluate the effective dispersion tensor through a computational analysis of the closure problem and associated laboratory measurements required to determine the sub-pore-scale parameters and geometry.

Different types of unit cell geometries have been used to calculate the effective dispersion tensor. For the first series of results, we used simple unit cells to describe the problem geometry. They allowed capturing significant features evident in more complex representations and significant insight can be gained on physical mechanisms involved. The effective dispersion tensor was determined for a wide range of dimensionless parameters, including the Péclet number, the biofilm volume fraction ε_ω and the normalized diffusivity $\mathscr{D}_\Gamma$. Our results suggest that these parameters, linked with the presence of the biofilm phase, have a strong impact on the calculation of $\mathbf{D}'_{eff}$.

Simple unit cells are known to provide reasonable qualitative behavior for dispersion problems, but poor quantitative results. In a first attempt to eliminate this limitation, we have solved the closure problems on three-dimensional realistically structured unit cells. For this latter need, high-resolution diffusion-weighted nuclear magnetic resonance microscopy for tomographic measurement of the distributions of the solid and fluid phases has been used. In spite of the difficulty to recover experimentally such geometry, we have been able to reconstruct the solid surface profile of a real porous medium in three dimensions whereas the biofilm phase was extrapolated from this reconstruction through a cellular automata model. Results have illustrated the impact of real porous medium complexity on the predicted tensor, especially at high Péclet numbers.

It must be emphasized that the use of our model is limited by the assumption of local mass equilibrium which is not always a valid assumption. Development of theoretical constraints and associated direct numerical simulations have helped us to identify the domain of validity which corresponds to $Pe_A < 1$ and $Da_A < 1$. Both approaches led to the same conclusion. To the best of our knowledge, this kind of constraint has not been clearly defined in previous models. In this context, calculations performed for the dispersion tensor show that a unit cell including only information at the lower scale about volume fractions is globally accurate enough to describe correctly the transport phenomenon within the framework of a local mass equilibrium assumption. In practice, this transport model, which ultimately needs to be coupled with a biofilm growth model if we are interested in studying the complete process of biodegradation, can be used for many applications as well as in natural attenuation of organic contaminants in aquifers than in wastewater biotreatment in packed bed reactors. However, given the constraints associated to the Péclet and Damköhler values involved, this formulation is particularly appropriate for groundwater systems where small characteristic pore sizes are present, and where typical velocities encountered are small so that the Péclet number constraint is met. The typical range of dimensionless numbers for this kind of system is presented in Dykaar and Kitanidis [15] and varies between 0.1 and 10^3 for the Péclet and between 0 and 10^4 for the Damköhler. As the Da_A value varies proportionally to the square of the pore dimension, the grain size is here a key parameter to determine whether such a model may be applied. If we consider for instance the classical scenario of biodegradation of TCE given as an example by Dykaar and Kitanidis [15], the consumption of this contaminant ($\mathscr{D}_{A\gamma} = 9.0 \cdot 10^{-6}$ cm^2/s) by a methanotrophic biofilm ($\rho_\omega = 0.03$ g/cm^3; $\mu_{A\omega} = 3.1 \cdot 10^{-5}$ s^{-1} and $K_{A\omega} = 4.2 \cdot 10^{-7}$ g/cm^3) in a coarse sand aquifer ($\ell_\gamma = 5 \cdot 10^{-2}$ cm with an average intrinsic velocity of $5 \cdot 10^{-4}$ cm/s) leads to values of 600 for Da_A and 2.8 for Pe_A. On the contrary, the same calculation but for a fine sand aquifer ($\ell_\gamma = 5 \cdot 10^{-3}$ cm) leads to Péclet and Damköhler values of 0.6 and 0.28, respectively, for which the LEA approximation is verified. This indicates that $Pe_A < 1$ and $Da_A < 1$ present somewhat severe restriction which do not apply in many relevant cases. This suggests that the development of non-equilibrium models would be a useful effort for the future studies [34,35].

In conclusion, this model establishes two separate but important goals:

1. It establishes via a formal upscaling procedure the proper form of the macroscale equations, and the associated domain of validity of the one-equation model. Additionally, the approach provides an explicit connection between the macroscale effective parameters that are identified with the structure of the microscale geometry and processes.
2. The approach provides a direct method for computing the effective macroscale parameters. When one has microscale geometric and process information for a representative unit volume, then one can compute unambiguously the effective parameters

that apply to the upscaled representation. The single largest difficulty in this computation is that it is not currently possible to tell *a priori* what volume constitutes a 'representative' one, and that 'representativeness' depends strongly upon the particular processes of interest. To address this problem, one must essentially conduct a kind of convergence analysis by adopting a set of increasingly complex unit cells, and then examine conditions for which the effective parameter no longer depends strongly upon additional complexity within the unit cell.

These two results are each useful, depending upon the intended purpose of the macroscale model that is developed. If one is interested only in establishing the proper form of the mass balance equation and the domain of validity, then no extensive closure problem needs to be solved. In essence, in this case, the parameters would be treated as being empirically measurable, but one at least has the confidence that the macroscale model that is adopted takes a self-consistent, proper form. In the second case, one hopes that some macroscale variables will be evidently highly correlated with the macroscale parameters. From this study, for example, the results suggest that the macroscale effective dispersion tensor is correlated strongly with the volume fraction of the biofilm and fluid phases, and with the correlation structure of the medium (i.e., the results from periodic and random media lead to different behaviors). The goal for this second approach is that ultimately a handful of such parameters can be established such that the effective dispersion tensor can be predicted with reasonable accuracy for a wide range of media. Although this study represents only an initial foray into the various kinds of media that might be encountered, it nonetheless lays out an approach which can be adopted in principle for any kind of structure within a representative volume characterized at the microscale.

Acknowledgements

This work has been partially supported by the EC2CO-CNRS/INSU program and the French Scientific Interest Group – Industrial Wasteland (GISFI), and by GdR 2990. B.D. Wood was supported in part by the National Science Foundation under Grant CBET 0449452 ('Microbial Transport and Adhesion – A Multiscale Approach') and the Department of Energy, Office of Science, Grant DE-PS02-07ER07-01. Paul Majors is thanked for providing MRI expertise in the measurement of the tomographic images of the porous media.

Appendix A. Development of the volume averaged equations

A.1. Averaging and simplifications

Although forming the volume average equations is conceptually straight forward, it does involve significant algebraic effort. We have provided the details of this development in this appendix. In Fig. 1, we have illustrated the three-phase system (biofilm, fluid, and solid) defining the microscale physical problem. The microscale equations are provided in the body of the paper, and are rewritten here for convenience

Biofilm phase

$$\frac{\partial c_{A\omega}}{\partial t} = \nabla\cdot(\mathbf{D}_{A\omega}\cdot\nabla c_{A\omega}) + R_{A\omega} \quad \text{in the } \omega\text{-phase}, \tag{A.1a}$$

$$\text{B.C.1} \qquad -\mathbf{n}_{\omega\kappa}\cdot\mathbf{D}_{A\omega}\cdot\nabla c_{A\omega} = 0 \quad \text{at } A_{\omega\kappa}, \tag{A.1b}$$

$$\text{B.C.2} \qquad -\mathbf{n}_{\gamma\kappa}\cdot\mathbf{D}_{A\gamma}\nabla c_{A\gamma} = 0 \quad \text{at } A_{\gamma\kappa}, \tag{A.1c}$$

$$\text{B.C.3} \qquad c_{A\gamma} = K_{A,eq}c_{A\omega} \quad \text{at } A_{\gamma\omega}, \tag{A.1d}$$

$$\text{B.C.4} \qquad -\mathbf{n}_{\omega\gamma}\cdot\mathbf{D}_{A\omega}\cdot\nabla c_{A\omega} = -\mathbf{n}_{\omega\gamma}\cdot\mathbf{D}_{A\gamma}\nabla c_{A\gamma} \quad \text{at } A_{\omega\gamma}, \tag{A.1e}$$

Fluid phase

$$\frac{\partial c_{A\gamma}}{\partial t} + \nabla\cdot(\mathbf{v}_{\gamma}c_{A\gamma}) = \nabla\cdot(\mathbf{D}_{A\gamma}\cdot\nabla c_{A\gamma}) \quad \text{in the } \gamma\text{-phase}. \tag{A.1f}$$

In Eq. (A.1a), $R_{A\omega}$ is the nonlinear reaction kinetic term

$$R_{A\omega} = -\mu_{A\omega}\rho_{\omega}\frac{c_{A\omega}}{c_{A\omega}+K_{A\omega}}\frac{c_{B\omega}}{c_{B\omega}+K_{B\omega}}. \tag{A.2}$$

In the developments that follow, we assume that within the averaging volume we can ignore variations in the parameters $\mathbf{D}_{A\omega}$, $\mathbf{D}_{A\gamma}$, $\mu_{A\omega}$, ρ_{ω}, $K_{A,\omega}$, $K_{B,\omega}$, and $K_{A,eq}$.

We wish to determine the macroscale transport equations that apply at the scale of the averaging volume illustrated in Fig. 1. To develop these expressions, we form the volume average of the two phases in which there is non-negligible transport. We begin by forming the superficial average of the transport equation for the ω-phase, Eq. (2), yielding

$$\left\langle\frac{\partial c_{A\omega}}{\partial t}\right\rangle = \langle\nabla\cdot(\mathbf{D}_{A\omega}\cdot\nabla c_{A\omega})\rangle + \langle R_{A\omega}\rangle. \tag{A.3}$$

For the system under study, microbial growth will create conditions where the surface of biofilm phase moves at a velocity **w** due to the increasing volume of the ω-phase. Under these conditions the *general transport theorem* [70] is required to interchange spatial integration and time differentiation,

General transport theorem

$$\left\langle\frac{\partial c_{A\omega}}{\partial t}\right\rangle = \frac{\partial\langle c_{A\omega}\rangle}{\partial t} - \frac{1}{\mathscr{V}}\int_{A_{\omega\gamma}(t)}\mathbf{n}_{\omega\gamma}\cdot\mathbf{w}c_{A\omega}\,dA \tag{A.4}$$

For interchanging spatial differentiation and integration, we need to make use of the *spatial averaging theorem* [24]. For three-phase systems, the averaging theorem takes the form [70]

Spatial averaging theorems

$$\langle\nabla c_{A\omega}\rangle = \nabla\langle c_{A\omega}\rangle + \frac{1}{\mathscr{V}}\int_{A_{\omega\gamma}(t)}\mathbf{n}_{\omega\gamma}c_{A\omega}\,dA + \frac{1}{\mathscr{V}}\int_{A_{\omega\kappa}(t)}\mathbf{n}_{\omega\kappa}c_{A\omega}\,dA, \tag{A.5}$$

$$\langle\nabla c_{A\gamma}\rangle = \nabla\langle c_{A\gamma}\rangle + \frac{1}{\mathscr{V}}\int_{A_{\gamma\omega}(t)}\mathbf{n}_{\gamma\omega}c_{A\gamma}\,dA + \frac{1}{\mathscr{V}}\int_{A_{\gamma\kappa}(t)}\mathbf{n}_{\gamma\kappa}c_{A\gamma}\,dA. \tag{A.6}$$

Applying Eqs. (A.4) and (A.5) to Eq. (A.3), we find

$$\begin{aligned}\frac{\partial\langle c_{A\omega}\rangle^{\omega}}{\partial t} = {}& \nabla\cdot\langle\mathbf{D}_{A\omega}\cdot\nabla c_{A}\rangle + \frac{1}{\mathscr{V}}\int_{A_{\omega\gamma}(t)}\mathbf{n}_{\omega\gamma}\cdot\mathbf{w}c_{A\omega}\,dA\\ &+\frac{1}{\mathscr{V}}\int_{A_{\omega\gamma}(t)}\mathbf{n}_{\omega\gamma}\cdot(\mathbf{D}_{A\omega}\cdot\nabla c_{A\omega})dA\\ &+\frac{1}{\mathscr{V}}\int_{A_{\omega\kappa}(t)}\mathbf{n}_{\omega\kappa}\cdot(\mathbf{D}_{A\omega}\cdot\nabla c_{A\omega})dA + \langle R_{A\omega}\rangle^{\omega}.\end{aligned} \tag{A.7}$$

Applying Eq. (A.5) a second time and using the definition of the intrinsic average ($\langle c_{A\omega}\rangle = \varepsilon_{\omega}\langle c_{A\omega}\rangle^{\omega}$) yields

$$\begin{aligned}\frac{\partial(\varepsilon_{\omega}\langle c_{A\omega}\rangle^{\omega})}{\partial t} = {}& \nabla\cdot\left[\mathbf{D}_{A\omega}\cdot\left(\varepsilon_{\omega}\nabla\langle c_{A\omega}\rangle^{\omega} + \langle c_{A\omega}\rangle^{\omega}\nabla\varepsilon_{\omega}\right.\right.\\ &\left.\left.+\frac{1}{\mathscr{V}}\int_{A_{\omega\gamma}(t)}\mathbf{n}_{\omega\gamma}c_{A\omega}\,dA + \frac{1}{\mathscr{V}}\int_{A_{\omega\kappa}(t)}\mathbf{n}_{\omega\kappa}c_{A\omega}\,dA\right)\right]\\ &+\frac{1}{\mathscr{V}}\int_{A_{\sigma\beta}(t)}\mathbf{n}_{\omega\gamma}\cdot\mathbf{w}c_{A\omega}\,dA\\ &+\frac{1}{\mathscr{V}}\int_{A_{\omega\gamma}(t)}\mathbf{n}_{\omega\gamma}\cdot(\mathbf{D}_{A\omega}\cdot\nabla c_{A\omega})dA\\ &+\frac{1}{\mathscr{V}}\int_{A_{\omega\kappa}(t)}\mathbf{n}_{\omega\kappa}\cdot(\mathbf{D}_{A\omega}\cdot\nabla c_{A\omega})dA + \varepsilon_{\omega}\langle R_{A\omega}\rangle^{\omega}.\end{aligned} \tag{A.8}$$

We will adopt two simplifications to the averaged transport equation for the ω-phase. The first is that the term involving convection

of the boundary can be neglected. Generally, the rate of biofilm growth will yield a boundary flux that is much smaller than the diffusive interfacial flux, i.e.,

$$\mathbf{n}_{\omega\gamma}\cdot\mathbf{w}c_{A\omega} \ll \mathbf{n}_{\omega\gamma}\cdot\mathbf{D}_{A\omega}\cdot\nabla c_{A\omega}, \tag{A.9}$$

or, in other words, the time-scale associated to the geometry evolution is much longer than the other physical and chemical process time scales. A similar restriction has been discussed in more detail by Wood and Whitaker [71]. The second simplification is that the nonlinear reaction term can be averaged to yield a result of the form

$$\langle R_{A\omega}\rangle^{\omega} = -\mu_{A\omega}\rho_{\omega}\frac{\langle c_{A\omega}\rangle^{\omega}}{\langle c_{A\omega}\rangle^{\omega}+K_{A\omega}}\frac{\langle c_{B\omega}\rangle^{\omega}}{\langle c_{B\omega}\rangle^{\omega}+K_{B\omega}}. \tag{A.10}$$

Although the reaction rate term is nonlinear, it is a particularly benign nonlinearity that is bounded by linear forms in the limits $\langle c_{A\omega}\rangle^{\omega} \ll K_{A\omega}$, $\langle c_{B\omega}\rangle^{\omega} \ll K_{B\omega}$ and $\langle c_{A\omega}\rangle^{\omega} \gg K_{A\omega}$, $\langle c_{B\omega}\rangle^{\omega} \gg K_{B\omega}$.

For this reason, the averaged reaction rate can be put in the form of Eq. (A.10) under the very mild restrictions. The development of Eq. (A.10) and the restrictions associated with its use are developed by Wood and Whitaker [73]. The simplified averaged transport equation takes the form

Averaged equation for the biofilm

$$\begin{aligned}\frac{\partial(\varepsilon_{\omega}\langle c_{A\omega}\rangle^{\omega})}{\partial t} = \nabla\cdot\Bigg[\mathbf{D}_{A\omega}\cdot\Bigg(&\varepsilon_{\omega}\nabla\langle c_{A\omega}\rangle^{\omega}+\langle c_{A\omega}\rangle^{\omega}\nabla\varepsilon_{\omega}\\ &+\frac{1}{\mathscr{V}}\int_{A_{\omega\gamma}(t)}\mathbf{n}_{\omega\gamma}c_{A\omega}\,dA+\frac{1}{\mathscr{V}}\int_{A_{\omega\kappa}(t)}\mathbf{n}_{\omega\kappa}c_{A\omega}\,dA\Bigg)\Bigg]\\ &+\frac{1}{\mathscr{V}}\int_{A_{\omega\gamma}(t)}\mathbf{n}_{\omega\gamma}\cdot(\mathbf{D}_{A\omega}\cdot\nabla c_{A\omega})dA\\ &+\frac{1}{\mathscr{V}}\int_{A_{\omega\kappa}(t)}\mathbf{n}_{\omega\kappa}\cdot(\mathbf{D}_{A\omega}\cdot\nabla c_{A\omega})dA\\ &-\varepsilon_{\omega}\mu_{A\omega}\rho_{\omega}\frac{\langle c_{A\omega}\rangle^{\omega}}{\langle c_{A\omega}\rangle^{\omega}+K_{A\omega}}\frac{\langle c_{B\omega}\rangle^{\omega}}{\langle c_{B\omega}\rangle^{\omega}+K_{B\omega}}.\end{aligned} \tag{A.11}$$

The same basic procedure can be followed to develop the average of Eq. (A.1e), yielding

$$\begin{aligned}\frac{\partial(\varepsilon_{\gamma}\langle c_{A\gamma}\rangle^{\gamma})}{\partial t}+\langle\nabla\cdot(\mathbf{v}_{\gamma}c_{A\gamma})\rangle = \nabla\cdot\Bigg[&\mathscr{D}_{A\gamma}\Big(\varepsilon_{\gamma}\nabla\langle c_{A\gamma}\rangle^{\gamma}+\langle c_{A\gamma}\rangle^{\gamma}\nabla\varepsilon_{\gamma}\\ &+\frac{1}{\mathscr{V}}\int_{A_{\omega\gamma}(t)}\mathbf{n}_{\gamma\omega}c_{A\gamma}\,dA\\ &+\frac{1}{\mathscr{V}}\int_{A_{\omega\kappa}(t)}\mathbf{n}_{\gamma\kappa}c_{A\gamma}\,dA\Big)\Bigg]\\ &+\frac{1}{\mathscr{V}}\int_{A_{\omega\gamma}(t)}\mathbf{n}_{\gamma\omega}\cdot(\mathscr{D}_{A\gamma}\nabla c_{A\gamma})dA\\ &+\frac{1}{\mathscr{V}}\int_{A_{\omega\kappa}(t)}\mathbf{n}_{\gamma\kappa}\cdot(\mathscr{D}_{A\gamma}\nabla c_{A\gamma})dA,\end{aligned} \tag{A.12}$$

Here we have imposed a constraint similar to the inequality (A.9)

$$\mathbf{n}_{\gamma\omega}\cdot\mathbf{w}c_{A\gamma} \ll \mathbf{n}_{\gamma\omega}\cdot\mathscr{D}_{A\gamma}\nabla c_{A\gamma}, \tag{A.13}$$

that allows us to neglect the convective flux that arises from the growth of the microbial phase.

The velocity term that appears in Eq. (A.12) requires some special treatment. First note that by the spatial average theorem

$$\begin{aligned}\langle\nabla\cdot(\mathbf{v}_{\gamma}c_{A\gamma})\rangle = \nabla\cdot\langle\mathbf{v}_{\gamma}c_{A\gamma}\rangle &+\frac{1}{\mathscr{V}}\int_{A_{\gamma\omega}(t)}\mathbf{n}_{\gamma\omega}\cdot\mathbf{v}_{\gamma}c_{A\gamma}\,dA\\ &+\frac{1}{\mathscr{V}}\int_{A_{\gamma\omega}(t)}\mathbf{n}_{\gamma\kappa}\cdot\mathbf{v}_{\gamma}c_{A\kappa}\,dA.\end{aligned} \tag{A.14}$$

Note that at the γ–κ and the γ–ω interfaces the normal convective flux is identically zero, allowing Eq. (A.14) to be simplified to

$$\langle\nabla\cdot(\mathbf{v}_{\gamma}c_{A\gamma})\rangle = \nabla\cdot\langle\mathbf{v}_{\gamma}c_{A\gamma}\rangle. \tag{A.15}$$

To simplify further, we define the spatial decompositions

$$\mathbf{v}_{\gamma} = \langle\mathbf{v}_{\gamma}\rangle^{\gamma}+\tilde{\mathbf{v}}_{\gamma}, \tag{A.16a}$$

$$c_{A\omega} = \langle c_{A\omega}\rangle^{\omega}+\tilde{c}_{A\omega}, \tag{A.16b}$$

$$c_{A\gamma} = \langle c_{A\gamma}\rangle^{\gamma}+\tilde{c}_{A\gamma}, \tag{A.16c}$$

so that

$$\nabla\cdot\langle\mathbf{v}_{\gamma}c_{A\gamma}\rangle = \nabla\cdot\langle\langle\mathbf{v}_{\gamma}\rangle^{\gamma}\langle c_{A\gamma}\rangle^{\gamma}+\tilde{\mathbf{v}}_{\gamma}\langle c_{A\gamma}\rangle^{\gamma}+\langle\mathbf{v}_{\gamma}\rangle^{\gamma}\tilde{c}_{A\gamma}+\tilde{\mathbf{v}}_{\gamma}\tilde{c}_{A\gamma}\rangle. \tag{A.17}$$

For the purposes of this analysis, we will impose the restrictions

$$\langle\tilde{\mathbf{v}}_{\gamma}\langle c_{A\gamma}\rangle^{\gamma}\rangle \ll \langle\tilde{\mathbf{v}}_{\gamma}\tilde{c}_{A\gamma}\rangle, \tag{A.18}$$

$$\langle\langle\mathbf{v}_{\gamma}\rangle^{\gamma}\tilde{c}_{A\gamma}\rangle \ll \langle\tilde{\mathbf{v}}_{\gamma}\tilde{c}_{A\gamma}\rangle. \tag{A.19}$$

These restrictions have been examined in more detail by Whitaker [70, Sections 3.2.1, 3.2.3, 3.3.1]. When this restriction is valid, Eq. (A.14) can be simplified to the form

$$\langle\nabla\cdot(\mathbf{v}_{\gamma}c_{A\gamma})\rangle = \nabla\cdot(\varepsilon_{\gamma}\langle\mathbf{v}_{\gamma}\rangle^{\gamma}\langle c_{A\gamma}\rangle^{\gamma})+\nabla\cdot\langle\tilde{\mathbf{v}}_{\gamma}\tilde{c}_{A\gamma}\rangle. \tag{A.20}$$

Substituting Eq. (A.20) into the volume averaged representation given in Eq. (A.12) yields

Averaged equation for the fluid

$$\begin{aligned}\underbrace{\frac{\partial(\varepsilon_{\gamma}\langle c_{A\gamma}\rangle^{\gamma})}{\partial t}}_{\text{Accumulation}}+\underbrace{\nabla\cdot(\varepsilon_{\gamma}\langle\mathbf{v}_{\gamma}\rangle^{\gamma}\langle c_{A\gamma}\rangle^{\gamma})}_{\text{Convection}} = &\underbrace{\nabla\cdot\Big[\mathbf{D}_{A\gamma}\Big(\varepsilon_{\gamma}\nabla\langle c_{A\gamma}\rangle^{\gamma}+\langle c_{A\gamma}\rangle^{\gamma}\nabla\varepsilon_{\gamma}+\frac{1}{\mathscr{V}}\int_{A_{\omega\gamma}(t)}\mathbf{n}_{\gamma\omega}c_{A\gamma}\,dA+\frac{1}{\mathscr{V}}\int_{A_{\omega\kappa}(t)}\mathbf{n}_{\gamma\kappa}c_{A\gamma}\,dA\Big)\Big]}_{\text{Diffusion}}\\ &+\underbrace{\frac{1}{\mathscr{V}}\int_{A_{\omega\gamma}(t)}\mathbf{n}_{\gamma\omega}\cdot(\mathbf{D}_{A\gamma}\nabla c_{A\gamma})dA+\frac{1}{\mathscr{V}}\int_{A_{\omega\kappa}(t)}\mathbf{n}_{\gamma\kappa}\cdot(\mathbf{D}_{A\gamma}\nabla c_{A\gamma})dA}_{\text{Interfacial Flux}}-\underbrace{\nabla\cdot\langle\tilde{\mathbf{v}}_{\gamma}\tilde{c}_{A\gamma}\rangle}_{\text{Dispersion}}.\end{aligned} \tag{A.21}$$

Eqs. (A.11) and (A.21) represent the volume averaged equations for the ω- and γ-phases, respectively. One difficulty with these expressions is that the microscale concentrations $c_{A\gamma}$ and $c_{A\omega}$ still appear on the right-hand side of the equation, so the equations are not yet closed (i.e., the independent variables are not yet expressed solely in terms of averages). Additionally, the equations are nonlocal in the sense of Cushman and Ginn [13]. We will discuss the method for closing the averaged equations in more detail below. First, however, we will examine the problem of nonlocality, and the constraints required to localize the transport equations.

A.2. Length-scale constraints for localisation

To eliminate the microscale concentration that appears in the area integrals in Eqs. (A.11) and (A.21), we decompose the concentration using Eq. (A.16). For example, for the first two area integrals on the right-hand side of Eq. (A.11) one finds

$$\frac{1}{\mathscr{V}}\int_{A_{\omega\gamma}(t)}\mathbf{n}_{\omega\gamma}c_{A\omega}\,dA+\frac{1}{\mathscr{V}}\int_{A_{\omega\kappa}(t)}\mathbf{n}_{\omega\kappa}c_{A\omega}\,dA$$
$$=\underbrace{\left\{\frac{1}{\mathscr{V}}\int_{A_{\omega\gamma}(t)}\mathbf{n}_{\omega\gamma}\langle c_{A\omega}\rangle^{\omega}\,dA+\frac{1}{\mathscr{V}}\int_{A_{\omega\kappa}(t)}\mathbf{n}_{\omega\kappa}\langle c_{A\omega}\rangle^{\omega}\,dA\right\}}_{\text{nonlocal terms}}$$
$$+\frac{1}{\mathscr{V}}\int_{A_{\omega\gamma}(t)}\mathbf{n}_{\omega\gamma}\tilde{c}_{A\omega}\,dA+\frac{1}{\mathscr{V}}\int_{A_{\omega\kappa}(t)}\mathbf{n}_{\omega\kappa}\tilde{c}_{A\omega}\,dA. \tag{A.22}$$

Eq. (A.22) still contains nonlocal terms because for any fixed point $\mathbf{x}$, the equation for the volume average will depend on upon averages at all points on $A_{\omega\gamma}$ and $A_{\omega\kappa}$ within the averaging volume. Under many circumstances, it may be valid to neglect the variation of the average concentration within the averaging volume. To develop explicit restrictions for these conditions, we expand the concentration $\langle c_{A\omega}\rangle^{\omega}$ in a Taylor series

$$\langle c_{A\omega}\rangle^{\omega}|_{\mathbf{x}+\mathbf{y}_{\omega}}=\langle c_{A\omega}\rangle^{\omega}|_{\mathbf{x}}+\mathbf{y}_{\omega}\cdot\nabla\langle c_{A\omega}\rangle^{\omega}|_{\mathbf{x}}$$
$$+\frac{1}{2}\mathbf{y}_{\omega}\mathbf{y}_{\omega}:\nabla\nabla\langle c_{A\omega}\rangle^{\omega}\Big|_{\mathbf{x}}+\cdots \tag{A.23}$$

Substituting this relation into Eq. (A.22) yields terms of the form

$$\left\{\frac{1}{\mathscr{V}}\int_{A_{\omega\gamma}(t)}\mathbf{n}_{\omega\gamma}\langle c_{A\omega}\rangle^{\omega}\,dA+\frac{1}{\mathscr{V}}\int_{A_{\omega\kappa}(t)}\mathbf{n}_{\omega\kappa}\langle c_{A\omega}\rangle^{\omega}\,dA\right\}$$
$$=\left\{\frac{1}{\mathscr{V}}\int_{A_{\omega\gamma}(t)}\mathbf{n}_{\omega\gamma}\,dA+\frac{1}{\mathscr{V}}\int_{A_{\omega\kappa}(t)}\mathbf{n}_{\omega\kappa}\,dA\right\}\langle c_{A\omega}\rangle^{\omega}|_{\mathbf{x}}$$
$$+\left\{\frac{1}{\mathscr{V}}\int_{A_{\omega\gamma}(t)}\mathbf{n}_{\omega\gamma}\mathbf{y}_{\omega}\,dA+\frac{1}{\mathscr{V}}\int_{A_{\omega\kappa}(t)}\mathbf{n}_{\omega\kappa}\mathbf{y}_{\omega}\,dA\right\}\cdot\nabla\langle c_{A\omega}\rangle^{\omega}\big|_{\mathbf{x}}+\cdots \tag{A.24}$$

Quintard and Whitaker [48] have provided a detailed analysis of the area integrals that appear on the right-hand side of Eq. (A.24). Their analysis suggests that the second and higher terms in the expansion are negligible relative to the first under the following constraints

$$\ell_{\omega}\ll R_0, \tag{A.25a}$$
$$R_0^2\ll L^2, \tag{A.25b}$$

where R_0 is the radius of the averaging volume, ℓ_{ω} is the characteristic length defining the microscale (e.g., the mean biofilm thickness), and L is the characteristic length defining the macroscale (e.g., the integral scale of the ω-phase indicator function). Assuming that these constraints are met, the second and higher terms in the expansion can be neglected relative to the first, and Eq. (A.22) takes the form (dropping the explicit notation of the dependence upon $\mathbf{x}$)

$$\frac{1}{\mathscr{V}}\int_{A_{\omega\gamma}(t)}\mathbf{n}_{\omega\gamma}c_{A\omega}\,dA+\frac{1}{\mathscr{V}}\int_{A_{\omega\kappa}(t)}\mathbf{n}_{\omega\kappa}c_{A\omega}\,dA$$
$$=\left\{\frac{1}{\mathscr{V}}\int_{A_{\omega\gamma}(t)}\mathbf{n}_{\omega\gamma}\,dA+\frac{1}{\mathscr{V}}\int_{A_{\omega\kappa}(t)}\mathbf{n}_{\omega\kappa}\,dA\right\}\langle c_{A\omega}\rangle^{\omega}$$
$$+\frac{1}{\mathscr{V}}\int_{A_{\omega\gamma}(t)}\mathbf{n}_{\omega\gamma}\tilde{c}_{A\omega}\,dA+\frac{1}{\mathscr{V}}\int_{A_{\omega\kappa}(t)}\mathbf{n}_{\omega\kappa}\tilde{c}_{A\omega}\,dA. \tag{A.26}$$

Finally, note that the averaging theorem can be used [by setting $c_{A\omega}=1$ in Eq. (A.5)] to show

$$\left\{\frac{1}{\mathscr{V}}\int_{A_{\omega\gamma}(t)}\mathbf{n}_{\omega\gamma}\,dA+\frac{1}{\mathscr{V}}\int_{A_{\omega\kappa}(t)}\mathbf{n}_{\omega\kappa}\,dA\right\}=-\nabla\varepsilon_{\omega}, \tag{A.27}$$

and use of this in Eq. (A.26) gives

$$\frac{1}{\mathscr{V}}\int_{A_{\omega\gamma}(t)}\mathbf{n}_{\omega\gamma}c_{A\omega}\,dA+\frac{1}{\mathscr{V}}\int_{A_{\omega\kappa}(t)}\mathbf{n}_{\omega\kappa}c_{A\omega}\,dA$$
$$=-\langle c_{A\omega}\rangle^{\omega}\nabla\varepsilon_{\omega}+\frac{1}{\mathscr{V}}\int_{A_{\omega\gamma}(t)}\mathbf{n}_{\omega\gamma}\tilde{c}_{A\omega}\,dA$$
$$+\frac{1}{\mathscr{V}}\int_{A_{\omega\kappa}(t)}\mathbf{n}_{\omega\kappa}\tilde{c}_{A\omega}\,dA. \tag{A.28}$$

A similar result holds for the γ-phase. When relation given by Eq. (A.28) is substituted in the conservation equation for $\langle c_{A\omega}\rangle^{\omega}$, Eq. (A.11), we obtain

Averaged equation for the biofilm (ω-phase)

$$\underbrace{\frac{\partial(\varepsilon_{\omega}\langle c_{A\omega}\rangle^{\omega})}{\partial t}}_{\text{Accumulation}}=\underbrace{\nabla\cdot\left[\varepsilon_{\omega}D_{A\omega}\cdot\left(\nabla\langle c_{A\omega}\rangle^{\omega}+\frac{1}{V_{\omega}}\int_{A_{\omega\gamma}(t)}\mathbf{n}_{\omega\gamma}\tilde{c}_{A\omega}\,dA+\frac{1}{V_{\omega}}\int_{A_{\omega\kappa}(t)}\mathbf{n}_{\omega\kappa}\tilde{c}_{A\omega}\,dA\right)\right]}_{\text{Diffusion}}$$
$$\times\underbrace{\frac{1}{\mathscr{V}}\int_{A_{\omega\gamma}(t)}\mathbf{n}_{\omega\gamma}\cdot(D_{A\omega}\cdot\nabla c_{A\omega})dA+\frac{1}{\mathscr{V}}\int_{A_{\omega\kappa}(t)}\mathbf{n}_{\omega\kappa}\cdot(D_{A\omega}\cdot\nabla c_{A\omega})dA}_{\text{Interfacial Flux}}+\underbrace{\varepsilon_{\omega}\langle R_{A\omega}\rangle^{\omega}}_{\text{Reaction}}, \tag{A.29}$$

and after a similar substitution in the conservation equation for $\langle c_{A\gamma}\rangle^{\gamma}$ we find

Averaged equation for the fluid (γ-phase, incompressible flow)

$$\underbrace{\frac{\partial(\varepsilon_\gamma\langle c_{A\gamma}\rangle^\gamma)}{\partial t}}_{\text{Accumulation}}+\underbrace{\varepsilon_\gamma\langle\mathbf{v}_\gamma\rangle^\gamma\cdot\nabla\langle c_{A\gamma}\rangle^\gamma}_{\text{Convection}}=\underbrace{\nabla\cdot\left[\varepsilon_\gamma\mathscr{D}_{A\gamma}\left(\nabla\langle c_{A\gamma}\rangle^\gamma+\frac{1}{V_\gamma}\int_{A_{\omega\gamma}(t)}\mathbf{n}_{\gamma\omega}\tilde{c}_{A\gamma}\,dA+\frac{1}{V_\gamma}\int_{A_{\omega\kappa}(t)}\mathbf{n}_{\gamma\kappa}\tilde{c}_{A\gamma}\,dA\right)\right]}_{\text{Diffusion}}$$
$$+\underbrace{\frac{1}{\mathscr{V}}\int_{A_{\omega\gamma}(t)}\mathbf{n}_{\gamma\omega}\cdot(\mathscr{D}_{A\gamma}\nabla c_{A\gamma})dA+\frac{1}{\mathscr{V}}\int_{A_{\omega\kappa}(t)}\mathbf{n}_{\gamma\kappa}\cdot(\mathscr{D}_{A\gamma}\nabla c_{A\gamma})dA}_{\text{Interfacial Flux}}-\underbrace{\nabla\cdot\langle\tilde{\mathbf{v}}_\gamma\tilde{c}_{A\gamma}\rangle}_{\text{Dispersive Transport}}\quad.\tag{A.30}$$

Here we have used the definitions

$$\varepsilon_\omega/V_\omega=1/\mathscr{V},\tag{A.31}$$
$$\varepsilon_\gamma/V_\gamma=1/\mathscr{V}.\tag{A.32}$$

Additionally, note that we have simplified the convection term in Eq. (A.30) by assuming that the flow field is incompressible, i.e.,

$$\nabla\cdot(\varepsilon_\gamma\langle\mathbf{v}_\gamma\rangle^\gamma)=0.\tag{A.33}$$

Eqs. (A.29) and (A.30) form the basis for our analysis of the one-equation model.

At this point, the fundamental discussion concerns the assumption of *local mass equilibrium* or *local mass non-equilibrium*. This issue is common to all reactive problems. Globally, two major classes of macroscopic models can be developed depending on the assumption made. If local mass equilibrium models have received a large attention in the past due their simplicity [e.g., Kansa et al. [25]; cf. Morales-Zarate et al. [37] for the application to a reactive three-phase system], specific precaution must be taken with reactive systems for which the assumption of small gradients is sometimes hard to verify [44,33]. Intrinsically, indeed, the presence of reactive source terms induce concentration gradients which can be more or less important. In the case of interest, however, given the large heterogeneity of kinetics and hydrodynamical parameters values encountered in real systems [15,67] leading to variations of several orders of magnitude of characteristic dimensionless numbers, such a simplified macroscale approach can be useful. A practical example of biodegradation *in situ* based on real data for which this assumption of local equilibrium can be considered, is be detailed in Section 7.

Appendix B. The closure problem

B.1. Derivation of the deviation conservation equations

To develop the governing differential equation for the deviation concentrations, we begin by subtracting the averaged equations from the point equations. For the development of the closure problem, we will neglect variations in *time* of the volume fractions ε_ω and ε_γ (this is consistent with our earlier assumption that the velocity of the biofilm–fluid interface could be neglected). In other words, we have posed the restrictions

$$\left|\langle c_{A\omega}\rangle^\omega\frac{\partial\varepsilon_\omega}{\partial t}\right|\ll\left|\varepsilon_\omega\frac{\partial\langle c_{A\omega}\rangle^\omega}{\partial t}\right|,\quad\left|\langle c_{A\gamma}\rangle^\gamma\frac{\partial\varepsilon_\gamma}{\partial t}\right|\ll\left|\varepsilon_\gamma\frac{\partial\langle c_{A\gamma}\rangle^\gamma}{\partial t}\right|\tag{B.1}$$

for the development of the closure problem. The resulting forms for the microscale and averaged equations are

Microscale equations

$$\frac{\partial c_{A\omega}}{\partial t}=\nabla\cdot(\mathbf{D}_{A\omega}\cdot\nabla c_{A\omega})+R_{A\omega}\quad\text{in the }\omega\text{-phase},\tag{B.2}$$
$$\frac{\partial c_{A\gamma}}{\partial t}+\mathbf{v}_\gamma\cdot\nabla c_{A\gamma}=\nabla\cdot(\mathbf{D}_{A\gamma}\cdot\nabla c_{A\gamma})\quad\text{in the }\gamma\text{-phase}.\tag{B.3}$$

Averaged equations

$$\begin{aligned}\frac{\partial\langle c_{A\omega}\rangle^\omega}{\partial t}&=\nabla\cdot(\mathbf{D}_{A\omega}\cdot\nabla\langle c_{A\omega}\rangle^\omega)+(\varepsilon_\omega^{-1}\nabla\varepsilon_\omega)\cdot(\mathbf{D}_{A\omega}\cdot\nabla\langle c_{A\omega}\rangle^\omega)\\&+\varepsilon_\omega^{-1}\nabla\cdot\left[\varepsilon_\omega\mathbf{D}_{A\omega}\cdot\left(\frac{1}{V_\omega}\int_{A_{\omega\gamma}(t)}\mathbf{n}_{\omega\gamma}\tilde{c}_{A\omega}\,dA+\frac{1}{V_\omega}\int_{A_{\omega\kappa}(t)}\mathbf{n}_{\omega\kappa}\tilde{c}_{A\omega}dA\right)\right]\\&+\varepsilon_\omega^{-1}\frac{1}{\mathscr{V}}\int_{A_{\omega\gamma}(t)}\mathbf{n}_{\omega\gamma}\cdot(\mathbf{D}_{A\omega}\cdot\nabla c_{A\omega})\,dA\\&+\varepsilon_\omega^{-1}\frac{1}{\mathscr{V}}\int_{A_{\omega\kappa}(t)}\mathbf{n}_{\omega\kappa}\cdot(\mathbf{D}_{A\omega}\cdot\nabla c_{A\omega})\,dA+\langle R_{A\omega}\rangle^\omega,\end{aligned}\tag{B.4}$$

$$\begin{aligned}\frac{\partial\langle c_{A\gamma}\rangle^\gamma}{\partial t}+\langle\mathbf{v}_\gamma\rangle^\gamma\cdot\nabla\langle c_{A\gamma}\rangle^\gamma&=\nabla\cdot(\mathscr{D}_{A\gamma}\nabla\langle c_{A\gamma}\rangle^\gamma)\\&+(\varepsilon_\gamma^{-1}\nabla\varepsilon_\gamma)\cdot(\mathscr{D}_{A\gamma}\nabla\langle c_{A\gamma}\rangle^\gamma)\\&+\varepsilon_\gamma^{-1}\nabla\cdot\left[\varepsilon_\gamma\mathscr{D}_{A\gamma}\left(\frac{1}{V_\gamma}\int_{A_{\omega\gamma}(t)}\mathbf{n}_{\gamma\omega}\tilde{c}_{A\gamma}\,dA\right.\right.\\&\left.\left.+\frac{1}{V_\gamma}\int_{A_{\omega\kappa}(t)}\mathbf{n}_{\gamma\kappa}\tilde{c}_{A\gamma}\,dA\right)\right]\\&+\varepsilon_\gamma^{-1}\frac{1}{\mathscr{V}}\int_{A_{\omega\gamma}(t)}\mathbf{n}_{\gamma\omega}\cdot(\mathscr{D}_{A\gamma}\nabla c_{A\gamma})\,dA\\&+\varepsilon_\gamma^{-1}\frac{1}{\mathscr{V}}\int_{A_{\omega\kappa}(t)}\mathbf{n}_{\gamma\kappa}\cdot(\mathscr{D}_{A\gamma}\nabla c_{A\gamma})\,dA\\&-\varepsilon_\gamma^{-1}\nabla\cdot\langle\tilde{\mathbf{v}}_\gamma\tilde{c}_{A\gamma}\rangle.\end{aligned}\tag{B.5}$$

Before continuing, note that we can make some simplifications to Eqs. (B.4) and (B.5). Note that in these equations area integrals that involve the microscale concentrations are still present. We can adopt the decompositions described in the main body of the paper, i.e. Eqs. (15) and (16), to express these integrals in terms of the average concentration. For example, in Eq. (B.4) we have

$$\begin{aligned}&\varepsilon_\omega^{-1}\frac{1}{\mathscr{V}}\left\{\int_{A_{\omega\gamma}(t)}\mathbf{n}_{\omega\gamma}\cdot(\mathbf{D}_{A\omega}\cdot\nabla c_{A\omega})\,dA+\int_{A_{\omega\kappa}(t)}\mathbf{n}_{\omega\kappa}\cdot(\mathbf{D}_{A\omega}\cdot\nabla c_{A\omega})\,dA\right\}\\&=\varepsilon_\omega^{-1}\frac{1}{\mathscr{V}}\left\{\int_{A_{\omega\kappa}(t)}\mathbf{n}_{\omega\kappa}\,dA+\int_{A_{\omega\gamma}(t)}\mathbf{n}_{\omega\gamma}\,dA\right\}\cdot(\mathbf{D}_{A\omega}\cdot\nabla\langle c_{A\omega}\rangle^\omega)\\&\quad+\varepsilon_\omega^{-1}\frac{1}{\mathscr{V}}\left\{\int_{A_{\omega\kappa}(t)}\mathbf{n}_{\omega\kappa}\cdot(\mathbf{D}_{A\omega}\cdot\nabla\tilde{c}_{A\omega})\,dA\right.\\&\quad\left.+\int_{A_{\omega\gamma}(t)}\mathbf{n}_{\omega\gamma}\cdot(\mathbf{D}_{A\omega}\cdot\nabla\tilde{c}_{A\omega})\,dA\right\}.\end{aligned}\tag{B.6}$$

Note that in this expression we have removed the average quantities from under the integrals as discussed in Appendix A (Section A.2). In Appendix A, we also developed the relationship

$$\left\{\frac{1}{\mathscr{V}}\int_{A_{\omega\gamma}(t)}\mathbf{n}_{\omega\gamma}\,dA+\frac{1}{\mathscr{V}}\int_{A_{\omega\gamma}(t)}\mathbf{n}_{\omega\gamma}\,dA\right\}=-\nabla\varepsilon_\omega,\tag{B.7}$$

and combining this with Eq. (B.6) yields

$$\varepsilon_\omega^{-1}\frac{1}{\mathscr{V}}\left\{\int_{A_{\omega\gamma}(t)}\mathbf{n}_{\omega\gamma}\cdot(\mathbf{D}_{A\omega}\cdot\nabla c_{A\omega})\,dA+\int_{A_{\omega\gamma}(t)}\mathbf{n}_{\omega\gamma}\cdot(\mathbf{D}_{A\omega}\cdot\nabla c_{A\omega})\,dA\right\}$$
$$=-\varepsilon_\omega^{-1}\nabla\varepsilon_\omega\cdot(\mathbf{D}_{A\omega}\cdot\nabla\langle c_{A\omega}\rangle^\omega)$$
$$+\varepsilon_\omega^{-1}\frac{1}{\mathscr{V}}\left\{\int_{A_{\omega\kappa}(t)}\mathbf{n}_{\omega\kappa}\cdot(\mathbf{D}_{A\omega}\cdot\nabla\tilde{c}_{A\omega})\,dA\right.$$
$$\left.+\int_{A_{\omega\gamma}(t)}\mathbf{n}_{\omega\gamma}\cdot(\mathbf{D}_{A\omega}\cdot\nabla\tilde{c}_{A\omega})\,dA\right\}. \tag{B.8}$$

Finally, substituting this result back into Eq. (B.4) gives the simplified averaged equation for the ω-phase

$$\frac{\partial\langle c_{A\omega}\rangle^\omega}{\partial t}=\nabla\cdot(\mathbf{D}_{A\omega}\cdot\nabla\langle c_{A\omega}\rangle^\omega)+\varepsilon_\omega^{-1}\nabla$$
$$\cdot\left[\varepsilon_\omega\mathbf{D}_{A\omega}\cdot\left(\frac{1}{V_\omega}\int_{A_{\omega\gamma}(t)}\mathbf{n}_{\omega\gamma}\tilde{c}_{A\omega}\,dA+\frac{1}{V_\omega}\int_{A_{\omega\kappa}(t)}\mathbf{n}_{\omega\kappa}\tilde{c}_{A\omega}\,dA\right)\right]$$
$$+\frac{1}{V_\omega}\int_{A_{\omega\gamma}(t)}\mathbf{n}_{\omega\gamma}\cdot(\mathbf{D}_{A\omega}\cdot\nabla\tilde{c}_{A\omega})\,dA$$
$$+\frac{1}{V_\omega}\int_{A_{\omega\kappa}(t)}\mathbf{n}_{\omega\kappa}\cdot(\mathbf{D}_{A\omega}\cdot\nabla\tilde{c}_{A\omega})\,dA+\langle R_{A\omega}\rangle^\omega. \tag{B.9}$$

A similar analysis for the γ-phase (Eq. (B.5)) gives

$$\frac{\partial\langle c_{A\gamma}\rangle^\gamma}{\partial t}+\mathbf{v}_\gamma\rangle^\gamma\cdot\nabla\langle c_{A\gamma}\rangle^\gamma=\nabla\cdot(\mathscr{D}_{A\gamma}\nabla\langle c_{A\gamma}\rangle^\gamma)$$
$$+\varepsilon_\gamma^{-1}\nabla\cdot\left[\varepsilon_\gamma\mathscr{D}_{A\gamma}\left(\frac{1}{V_\gamma}\int_{A_{\omega\gamma}(t)}\mathbf{n}_{\gamma\omega}\tilde{c}_{A\gamma}\,dA\right.\right.$$
$$\left.\left.+\frac{1}{V_\gamma}\int_{A_{\omega\kappa}(t)}\mathbf{n}_{\gamma\kappa}\tilde{c}_{A\gamma}\,dA\right)\right]$$
$$+\frac{1}{V_\gamma}\int_{A_{\omega\gamma}(t)}\mathbf{n}_{\gamma\omega}\cdot(\mathscr{D}_{A\gamma}\nabla\tilde{c}_{A\gamma})\,dA$$
$$+\frac{1}{V_\gamma}\int_{A_{\omega\kappa}(t)}\mathbf{n}_{\gamma\kappa}\cdot(\mathscr{D}_{A\gamma}\nabla\tilde{c}_{A\gamma})\,dA$$
$$-\varepsilon_\gamma^{-1}\nabla\cdot\langle\tilde{\mathbf{v}}_\gamma\tilde{c}_{A\gamma}\rangle. \tag{B.10}$$

To develop conservation equations for the deviation quantities we subtract the macroscale equation from the microscale equation. Subtracting Eq. (B.9) from Eq. (B.2) and Eq. (B.10) from Eq. (B.3) generates deviation equations that take the form

Deviation equation – biofilm phase

$$\frac{\partial\tilde{c}_{A\omega}}{\partial t}=\nabla\cdot(\mathbf{D}_{A\omega}\cdot\nabla\tilde{c}_{A\omega})-\varepsilon_\omega^{-1}\nabla$$
$$\cdot\left[\varepsilon_\omega\mathbf{D}_{A\omega}\cdot\left(\frac{1}{V_\omega}\int_{A_{\omega\gamma}(t)}\mathbf{n}_{\omega\gamma}\tilde{c}_{A\omega}\,dA+\frac{1}{V_\omega}\int_{A_{\omega\kappa}(t)}\mathbf{n}_{\omega\kappa}\tilde{c}_{A\omega}\,dA\right)\right]$$
$$-\frac{1}{V_\omega}\int_{A_{\omega\gamma}(t)}\mathbf{n}_{\omega\gamma}\cdot(\mathbf{D}_{A\omega}\cdot\nabla\tilde{c}_{A\omega})\,dA$$
$$-\frac{1}{V_\omega}\int_{A_{\omega\kappa}(t)}\mathbf{n}_{\omega\kappa}\cdot(\mathbf{D}_{A\omega}\cdot\nabla\tilde{c}_{A\omega})\,dA+(R_{A\omega}-\langle R_{A\omega}\rangle^\omega), \tag{B.11}$$

Deviation equation – fluid-phase

$$\frac{\partial\tilde{c}_{A\gamma}}{\partial t}+\nabla\cdot(\mathbf{v}_\gamma c_{A\gamma})-\langle\mathbf{v}_\gamma\rangle^\gamma\cdot\nabla\langle c_{A\gamma}\rangle^\gamma$$
$$=\nabla\cdot(\mathscr{D}_{A\gamma}\nabla\tilde{c}_{A\gamma})$$
$$-\varepsilon_\gamma^{-1}\nabla\cdot\left[\varepsilon_\gamma\mathscr{D}_{A\gamma}\left(\frac{1}{V_\gamma}\int_{A_{\omega\gamma}(t)}\mathbf{n}_{\gamma\omega}\tilde{c}_{A\gamma}\,dA+\frac{1}{V_\gamma}\int_{A_{\omega\kappa}(t)}\mathbf{n}_{\gamma\kappa}\tilde{c}_{A\gamma}\,dA\right)\right]$$
$$-\frac{1}{V_\gamma}\int_{A_{\omega\gamma}(t)}\mathbf{n}_{\gamma\omega}\cdot(\mathscr{D}_{A\gamma}\nabla\tilde{c}_{A\gamma})\,dA$$
$$-\frac{1}{V_\gamma}\int_{A_{\omega\kappa}(t)}\mathbf{n}_{\gamma\kappa}\cdot(\mathscr{D}_{A\gamma}\nabla\tilde{c}_{A\gamma})\,dA+\varepsilon_\gamma^{-1}\nabla\cdot\langle\tilde{\mathbf{v}}_\gamma\tilde{c}_{A\gamma}\rangle. \tag{B.12}$$

Although Eqs. (B.11) and (B.12) are complex, these expressions can be additionally simplified. To begin with, we note that the reaction deviation term is generally negligible relative to the diffusive term

$$(R_{A\omega}-\langle R_{A\omega}\rangle^\omega)\ll\nabla\cdot(\mathbf{D}_{A\omega}\cdot\nabla\tilde{c}_{A\omega}). \tag{B.13}$$

A restriction for this has been developed by Wood and Whitaker [73], and takes the form

$$\frac{\mathbf{D}_{A\omega}}{\ell_\omega}\gg\left(\frac{\mu_{A\omega}}{K_{A\omega}}\frac{\tilde{c}_{A\gamma}}{\tilde{c}_{B\gamma}}\right). \tag{B.14}$$

Further estimates for the deviation terms that appear in this restriction can be found by following developments similar to those of Wood and Whitaker [71]. For this work, we will assume that the restriction given by Eq. (B.14) is valid.

For the γ-phase note that using the decompositions given by Eqs. (A.16a) and (A.16c), the microscale convection term can be put in the form

$$\nabla\cdot(\mathbf{v}_\gamma c_{A\gamma})=\mathbf{v}_\gamma\cdot\nabla c_{A\gamma}=(\langle\mathbf{v}_\gamma\rangle^\gamma+\tilde{\mathbf{v}}_\gamma)\cdot(\nabla\langle c_{A\gamma}\rangle^\gamma+\nabla\tilde{c}_{A\gamma})$$
$$=\langle\mathbf{v}_\gamma\rangle^\gamma\cdot\nabla\langle c_{A\gamma}\rangle^\gamma+\tilde{\mathbf{v}}_\gamma\cdot\nabla\langle c_{A\gamma}\rangle^\gamma+\mathbf{v}_\gamma\cdot\nabla\tilde{c}_{A\gamma}. \tag{B.15}$$

Use of this result in Eq. (B.12) gives

$$\frac{\partial\tilde{c}_{A\gamma}}{\partial t}+\tilde{\mathbf{v}}_\gamma\cdot\nabla\langle c_{A\gamma}\rangle^\gamma+\mathbf{v}_\gamma\cdot\nabla\tilde{c}_{A\gamma}$$
$$=\nabla\cdot(\mathscr{D}_{A\gamma}\nabla\tilde{c}_{A\gamma})-\varepsilon_\gamma^{-1}\nabla$$
$$\cdot\left[\varepsilon_\gamma\mathscr{D}_{A\gamma}\left(\frac{1}{V_\gamma}\int_{A_{\omega\gamma}(t)}\mathbf{n}_{\gamma\omega}\tilde{c}_{A\gamma}\,dA+\frac{1}{V_\gamma}\int_{A_{\omega\kappa}(t)}\mathbf{n}_{\gamma\kappa}\tilde{c}_{A\gamma}\,dA\right)\right]$$
$$-\frac{1}{V_\gamma}\int_{A_{\omega\gamma}(t)}\mathbf{n}_{\gamma\omega}\cdot(\mathscr{D}_{A\gamma}\nabla\tilde{c}_{A\gamma})\,dA-\frac{1}{V_\gamma}\int_{A_{\omega\kappa}(t)}\mathbf{n}_{\gamma\kappa}$$
$$\cdot(\mathscr{D}_{A\gamma}\nabla\tilde{c}_{A\gamma})\,dA+\varepsilon_\gamma^{-1}\nabla\cdot\langle\tilde{\mathbf{v}}_\gamma\tilde{c}_{A\gamma}\rangle. \tag{B.16}$$

When the decompositions given by Eqs. (A.16a)–(A.16d) are used with the boundary conditions given by Eqs. (3)–(6) and adopting the simplifications described above, the closure problem can be stated as

Closure problem

$$\frac{\partial\tilde{c}_{A\omega}}{\partial t}=\nabla\cdot(\mathbf{D}_{A\omega}\cdot\nabla\tilde{c}_{A\omega})-\varepsilon_\omega^{-1}\nabla$$
$$\cdot\left[\varepsilon_\omega\mathbf{D}_{A\omega}\cdot\left(\frac{1}{V_\omega}\int_{A_{\omega\gamma}(t)}\mathbf{n}_{\omega\gamma}\tilde{c}_{A\omega}\,dA+\frac{1}{V_\omega}\int_{A_{\omega\kappa}(t)}\mathbf{n}_{\omega\kappa}\tilde{c}_{A\omega}\,dA\right)\right]$$
$$-\frac{1}{V_\omega}\int_{A_{\omega\gamma}(t)}\mathbf{n}_{\omega\gamma}\cdot(\mathbf{D}_{A\omega}\cdot\nabla\tilde{c}_{A\omega})\,dA-\frac{1}{V_\omega}\int_{A_{\omega\kappa}(t)}\mathbf{n}_{\omega\kappa}$$
$$\cdot(\mathbf{D}_{A\omega}\cdot\nabla\tilde{c}_{A\omega})\,dA, \tag{B.17a}$$

B.C.1
$$-\mathbf{n}_{\omega\kappa}\cdot\mathbf{D}_{A\omega}\cdot\nabla\tilde{c}_{A\omega}=\underbrace{\mathbf{n}_{\omega\kappa}\cdot K_{A,eq}^{-1}\mathbf{D}_{A\omega}\cdot\nabla\{c_A\}}_{\text{dispersive source}}\quad\text{at } A_{\omega\kappa}, \tag{B.17b}$$

B.C.2
$$-\mathbf{n}_{\gamma\kappa}\cdot\mathscr{D}_{A\gamma}\nabla\tilde{c}_{A\gamma}=\underbrace{\mathbf{n}_{\gamma\kappa}\cdot\mathscr{D}_{A\gamma}\nabla\{c_A\}}_{\text{dispersive source}},\quad\text{at } A_{\gamma\kappa}, \tag{B.17c}$$

B.C.3
$$\tilde{c}_{A\gamma}=K_{A,eq}\tilde{c}_{A\omega},\quad\text{at } A_{\gamma\omega}, \tag{B.17d}$$

B.C.4
$$\mathbf{n}_{\gamma\omega}\cdot\mathbf{D}_{A\omega}\cdot\nabla\tilde{c}_{A\omega}=\mathbf{n}_{\gamma\omega}\cdot\mathscr{D}_{A\gamma}\nabla\tilde{c}_{A\gamma}$$
$$+\underbrace{\mathbf{n}_{\gamma\omega}\cdot(\mathbf{I}\mathscr{D}_{A\gamma}-K_{A,eq}^{-1}\mathbf{D}_{A\omega})\cdot\nabla\{c_A\}}_{\text{dispersive source}}$$
$$\text{at } A_{\gamma\omega}, \tag{B.17e}$$

$$\frac{\partial \tilde{c}_{A\gamma}}{\partial t} + \tilde{\mathbf{v}}_\gamma \cdot \nabla \langle c_{A\gamma}\rangle^\gamma + \mathbf{v}_\gamma \cdot \nabla \tilde{c}_{A\gamma}$$
$$= \nabla \cdot (\mathscr{D}_{A\gamma} \nabla \tilde{c}_{A\gamma}) - \varepsilon_\gamma^{-1} \nabla$$
$$\cdot \left[\varepsilon_\gamma \mathscr{D}_{A\gamma} \left(\frac{1}{V_\gamma} \int_{A_{\omega\gamma}(t)} \mathbf{n}_{\gamma\omega} \tilde{c}_{A\gamma}\, dA + \frac{1}{V_\gamma} \int_{A_{\omega\kappa}(t)} \mathbf{n}_{\gamma\kappa} \tilde{c}_{A\gamma}\, dA \right) \right]$$
$$- \frac{1}{V_\gamma} \int_{A_{\omega\gamma}(t)} \mathbf{n}_{\gamma\omega} \cdot \left(\mathscr{D}_{A\gamma} \nabla \tilde{c}_{A\gamma} \right) dA - \frac{1}{V_\gamma} \int_{A_{\omega\kappa}(t)} \mathbf{n}_{\gamma\kappa}$$
$$\cdot \left(\mathscr{D}_{A\gamma} \nabla \tilde{c}_{A\gamma} \right) dA + \varepsilon_\gamma^{-1} \nabla \cdot \langle \tilde{\mathbf{v}}_\gamma \tilde{c}_{A\gamma} \rangle. \tag{B.17f}$$

For the boundary conditions we have assumed that local mass equilibrium is valid

$$\langle c_{A\gamma}\rangle^\gamma = K_{A,eq} \langle c_{A\omega}\rangle^\omega = \{c_A\}. \tag{B.18}$$

B.2. Derivation of the deviation conservation equations

$$\tilde{c}_{A\gamma} = \mathbf{b}_{A\gamma} \cdot \nabla \{c_A\}, \tag{B.19}$$
$$K_{A,eq} \tilde{c}_{A\omega} = \mathbf{b}_{A\omega} \cdot \nabla \{c_A\}. \tag{B.20}$$

Closure problem

$$0 = \nabla \cdot (\mathbf{D}_{A\omega} \cdot \nabla \mathbf{b}_{A\omega}) - \frac{1}{V_\omega} \int_{A_{\omega\gamma}(t)} \mathbf{n}_{\omega\gamma} \cdot (\mathbf{D}_{A\omega} \cdot \nabla \mathbf{b}_{A\omega})\, dA$$
$$- \frac{1}{V_\omega} \int_{A_{\omega\kappa}(t)} \mathbf{n}_{\omega\kappa} \cdot (\mathbf{D}_{A\omega} \cdot \nabla \mathbf{b}_{A\omega})\, dA, \tag{B.21a}$$

B.C.1
$$- \mathbf{n}_{\omega\kappa} \cdot D_{A\omega} \cdot \nabla \mathbf{b}_{A\omega} = \underbrace{\mathbf{n}_{\omega\kappa} \cdot \mathbf{D}_{A\omega}}_{\text{dispersive source}} \quad \text{at } A_{\omega\kappa}, \tag{B.21b}$$

B.C.2
$$- \mathbf{n}_{\gamma\kappa} \cdot \mathscr{D}_{A\gamma} \nabla \mathbf{b}_{A\gamma} = \underbrace{\mathbf{n}_{\gamma\kappa} \mathscr{D}_{A\gamma}}_{\text{dispersive source}}, \quad \text{at } A_{\gamma\kappa}, \tag{B.21c}$$

B.C.3
$$\mathbf{b}_{A\gamma} = \mathbf{b}_{A\omega}, \quad \text{at } A_{\gamma\omega}, \tag{B.21d}$$

B.C.4
$$\mathbf{n}_{\gamma\omega} \cdot \mathbf{D}_{A\omega} \cdot \nabla \mathbf{b}_{A\omega} = \mathbf{n}_{\gamma\omega} \cdot K_{A,eq} \mathscr{D}_{A\gamma} \nabla \mathbf{b}_{A\gamma} + \underbrace{\mathbf{n}_{\gamma\omega} \cdot (K_{A,eq} \mathbf{I} \mathscr{D}_{A\gamma} - \mathbf{D}_{A\omega})}_{\text{dispersive source}} \quad \text{at } A_{\gamma\omega}, \tag{B.21e}$$

$$\tilde{\mathbf{v}}_\gamma + \mathbf{v}_\gamma \cdot \nabla \mathbf{b}_{A\gamma} = \mathscr{D}_{A\gamma} \nabla^2 \mathbf{b}_{A\gamma} - \frac{\mathscr{D}_{A\gamma}}{V_\gamma} \left\{ \int_{A_{\omega\gamma}(t)} \mathbf{n}_{\gamma\omega} \cdot \nabla \mathbf{b}_{A\gamma} dA + \int_{A_{\omega\kappa}(t)} \mathbf{n}_{\gamma\kappa} \cdot \nabla \mathbf{b}_{A\gamma} dA \right\}, \tag{B.21f}$$

Periodicity

$$\mathbf{b}_{A\gamma}(\mathbf{r}) = \mathbf{b}_{A\gamma}(\mathbf{r} + \mathbf{l}_i), \tag{B.21g}$$
$$\mathbf{b}_{A\omega}(\mathbf{r}) = \mathbf{b}_{A\omega}(\mathbf{r} + \mathbf{l}_i). \tag{B.21h}$$

References

[1] Ahmadi A, Quintard M. Large-scale properties for two-phase flow in random porous media. J Hydrol 1996;183(1–2):69–99.
[2] Ahmadi A, Aigueperse A, Quintard M. Calculation of the effective properties describing active dispersion in porous media: from simple to complex unit cells. Adv Water Resour 2001;24:431–8.
[3] Aris R. On the dispersion of a solute in a fluid flowing through a tube. Proc R Soc Lond A 1956;235:67–77.
[4] Aspa Y, Debenest G, Quintard M. Effective dispersion in channeled biofilms. Int J Environ Waste Manage, in press.
[5] Baveye P, Valocchi AJ. An evaluation of mathematical models of the transport of biologically reacting solutes in saturated soils and aquifers. Water Resour Res 1989;25(6):1413–21.
[6] Borden RC, Bedient PB. Transport of dissolved hydrocarbons influenced by oxygen-limited biodegradation. 1: Theoretical development. Water Resour Res 1986;22:1973–82.
[7] Borden RC, Bedient PB, Lee MD, Ward CH, Wilson JT. Transport of dissolved hydrocarbons influenced by oxygen-limited biodegradation. 2: Field application. Water Resour Res 1986;22:1983–90.
[8] Chen Y-M, Abriola LM, Alvarez PJJ, Anid PJ, Vogel TM. Modeling transport and biodegradation of benzene and toluene in sandy aquifer material: comparison with experimental measurements. Water Resour Res 1992;28:1833–47.
[9] Chrysikopoulos CV, Kitanidis PK, Roberts PV. Generalized Taylor–Aris moment analysis of the transport of sorbing solutes through porous media with spatially-periodic retardation factor. Trans Porous Media 1992;7(2):163–85.
[10] Cirpka OA, Frind EO, Helmig R. Numerical simulation of biodegradation controlled by transverse mixing. J Contam Hydrol 1999;40:159–82.
[11] Cushman JH. On the unifying concepts of scale, instrumentation, and stochastics in the development of multiphase transport theory. Water Resour Res 1984;20:1668–76.
[12] Cushman JH, editor. Dynamics of Fluids in Hierarchical Porous Media. San Diego (CA): Academic; 1990.
[13] Cushman JH, Ginn TR. Nonlocal dispersion in media with continuously evolving scales of heterogeneity. Trans Porous Media 1993;13:123–38.
[14] de Blanc P, McKinney D, Speitel G. Modeling subsurface biodegradation of non-aqueous phase liquids. In: Corapcioglu Y, editor. Advances in porous media, vol. 3. Amsterdam, The Netherlands: Elsevier; 1996. p. 1–86.
[15] Dykaar BB, Kitanidis PK. Macrotransport of a biologically reacting solute through porous media. Water Resour Res 1996;32(2):307–20.
[16] Eames I, Bush JWM. Longitudinal dispersion by bodies fixed in a potential flow. Proc R Soc Lond A 1999;455:3665–86.
[17] Eberl HJ, Picioreanu C, Heijnen JJ, van Loosdrecht MCM. A three-dimensional numerical study on the correlation of spatial structure, hydrodynamic conditions, and mass transfer and conversion in biofilms. Chem Eng Sci 2000;55:6209–22.
[18] Ginn TR, Wood BD, Nelson KE, Scheibe TD, Murphy EM, Clement TP. Processes in microbial transport in the natural subsurface. Adv Water Resour 2002;25:1017–42.
[19] Glowinski R. Numerical methods for nonlinear variational problems. New York (NY, USA): Springer-Verlag; 1984.
[20] Golfier F, Zarcone C, Bazin B, Lenormand R, Lasseux D, Quintard M. Modelling of the dissolution in porous media at the Darcy-scale: on the ability of a Darcy-scale model to capture wormhole formation during the dissolution of a porous medium. J Fluid Mech 2002;457:213–54.
[21] Gray WG, Leijnse A, Kolar RL, Blain CA. Mathematical tools for changing spatial scales in the analysis of physical systems. Boca Raton (FL): CRC Press; 1993.
[22] Hadden DA, Rill RL, McFaddan L, Locke BR. Oligonucleotide and water self-diffusion in systems of pluronic triblock copolymers and in buffer solutions by pulsed field gradient nuclear magnetic resonance. Macromolecules 2000;33(11):4235–48.
[23] Hornung U. Homogenization and porous media. Interdisciplinary applied mathematics series 6. New York: Springer-Verlag; 1997.
[24] Howes FA, Whitaker S. The spatial averaging theorem revisited. Chem Eng Sci 1985;40:1387–92.
[25] Kansa E, Perler H, Chaiken R. Mathematical model of wood pyrolysis including internal forced convection. Combust Flame 1977;29:311–24.
[26] Kim S, Corapcioglu Y. The role of biofilm growth in bacteria-facilitated contaminant transport in porous media. Trans Porous Media 1997;26:161–81.
[27] Kinzelbach W, Schäfer W, Herzer J. Numerical modeling of natural and enhanced denitrification processes in aquifers. Water Resour Res 1991;27(6):1123–35.
[28] Knutson C, Valocchi A, Werth C. Comparison of continuum and pore-scale models of nutrient biodegradation under transverse mixing conditions. Adv Water Resour 2006;30(6–7):1421–31. doi:10.1016/j.advwatres.2006.05.012.
[29] Lasseux D, Ahmadi A, Cleis X, Garnier J. A macroscopic model for species transport during in vitro tissue growth obtained by the volume averaging method. Chem Eng Sci 2004;59:1949–64.
[30] Majors PD, McLean JS, Fredrickson JK, Wind RA. NMR methods for in situ biofilm metabolism studies: spatial and temporal resolved measurements. Water Sci Technol 2005;52(7):7–12.
[31] Maxwell JC. A treatise on electricity and magnetism. 3rd ed. (reproduction of Claridon Press imprint). New York: Dover Publications; 1873.
[32] Megee RD, Kinoshita S, Fredrickson AG, Tsuchiya HM. Differentiation and product formation in molds. Biotechnol Bioeng 1970;12:771–801.
[33] Mermoud F, Golfier F, Salvador S, Van de Steene L. Experimental and numerical study of steam gasification of a single charcoal particle. Combust Flame 2006;145(1–2):59–79.
[34] Mikelic A, Devigne V, Van Duijn CJ. Rigorous upscaling of the reactive flow through a pore, under dominant Peclet and Damkohler numbers. SIAM J Math Anal 2006;38:1262–87.
[35] Mikelic A, Rosier C. Rigorous upscaling of the infinite adsorption rate reactive flow under dominant Peclet number through a pore. Ann Univ Ferrara 2007;53:333–59.
[36] Miller MA, Allen DG. Transport of hydrophobic pollutants through biofilms and biofilters. Chem Eng Sci 2004;59:3515–25.

[37] Morales-Zarate E, Valdes-Parada FJ, Goyeau B, Ochoa-Tapia JA. Diffusion and reaction in three-phase systems: average transport equations and jump boundary conditions. Chem Eng Sci 2008;138:307–22.
[38] Murphy EM, Ginn TR. Modeling microbial processes in porous media. Hydrogeol J 2000;8:142–58.
[39] Ochoa JA, Stroeve P, Whitaker S. Diffusion and reaction in cellular media. Chem Eng Sci 1986;41:2999–3013.
[40] Ochoa-Tapia JA, Stroeve P, Whitaker S. Diffusive transport in two-phase media: spatially periodic models and Maxwell's theory for isotropic and anisotropic systems. Chem Eng Sci 1994;49:709–26.
[41] Picioreanu C, Van Loosdrecht MCM, Heijnen JJ. Mathematical modeling of biofilm structure with a hybrid differential-discrete cellular automaton approach. Biotechnol Bioeng 1998;58(1):101–16.
[42] Picioreanu C, Van Loosdrecht MCM, Heijnen JJ. Effect of diffusive and convective substrate transport on biofilm structure formation: a two-dimensional modeling study. Biotechnol Bioeng 2000;69(5):504–15.
[43] Pickup GE, Ringrose PS, Jensen JL, Sorbie K. Permeability tensors for sedimentary structures. Math Geol 1994;26:227–50.
[44] Puiroux N, Prat M, Quintard M. Non-equilibrium theories for macroscale heat transfer: ablative composite layer systems. Int J Therm Sci 2004;43(6):541–54.
[45] Quintard M. Diffusion in isotropic and anisotropic porous systems: three-dimensional calculations. Trans Porous Media 1993;11:187–99.
[46] Quintard M, Whitaker S. Transport in ordered and disordered porous media: volume-averaged equations, closure problems and comparison with experiment. Chem Eng Sci 1993;48(14):2537–64.
[47] Quintard M, Whitaker S. Advances in heat transfer. New York: Academic Press; 1993. p. 369–464.
[48] Quintard M, Whitaker S. Convection, dispersion, and interfacial transport of contaminants: homogeneous porous media. Adv Water Resour 1994;17:221–39.
[49] Quintard M, Kaviany M, Whitaker S. Two medium treatment of heat transfer in porous media: numerical results for effective properties. Adv Water Resour 1997;20(2–3):77–94.
[50] Rayleigh Lord (John William Strutt). On the influence of obstacles arranged in rectangular order upon the properties of the medium. Philos Mag 1892;34:481–9.
[51] Renard P, de Marsily G. Calculating equivalent permeability: a review. Adv Water Resour 1997;20:253–78.
[52] Rittmann BE. The significance of biofilms in porous media. Water Resour Res 1993;29(7):2195–202.
[53] Roels JA. Energetics and kinetics in biotechnology. Amsterdam: Elsevier; 1983.
[54] Semprini L, McCarty PL. Comparison between model simulations and field results for in situ biorestoration of chlorinated aliphatics. Part 1: Biostimulation of methanotrophic bacteria. Ground Water 1991;29:365–74.
[55] Seymour JD, Gage JP, Codd SL, Gerlach R. Magnetic resonance microscopy of biofouling induced scale dependent transport in porous media. Adv Water Resour 2007;30:1408–20.
[56] Seymour JD, Codd SL, Gjersing EL, Stewart PS. Magnetic resonance microscopy of biofilm structure and impact on transport in a capillary bioreactor. J Magn Reson 2004;167:322–7.
[57] Shafahi M, Vafai K. Biofilm affected characteristics of porous structures. Int J Heat Mass Transfer 2008. doi:10.1016/j.ijheatmasstransfer.2008.07.013.
[58] Skowlund CT. Effect of biofilm growth on steady-state biofilm models. Biotechnol Bioeng 1990;35(5):502–10.
[59] Souto HPA, Moyne C. Dispersion in two-dimensional periodic porous media. Part II: Dispersion tensor. Phys Fluids 1997;9:2253–63.
[60] Stewart PS. A review of experimental measurements of effective diffusive permeabilities and effective diffusion coefficients in biofilms. Biotechnol Bioeng 1998;59(3):261–72.
[61] Sykes JF, Soyupak S, Farquhar GJ. Modeling of leachate organic migration and attenuation in groundwaters below sanitary landfills. Water Resour Res 1982;18:135–45.
[62] Taylor SG. Dispersion of soluble matter in solvent flowing slowly through a tube. Proc R Soc Lond 1953;219:186–203.
[63] Taylor S, Jaffe P. Substrate and biomass transport in a porous medium. Water Resour Res 1990;26(9):2181–94.
[64] Thullner M, Mauclaire L, Schroth MH, Kinzelbach W, Zeyer J. Interaction between water flow and spatial distribution of microbial growth in a two-dimensional flow field in saturated porous media. J Contam Hydrol 2002;58:169–89.
[65] Valocchi A. Validity of the local equilibrium assumption for modeling sorbing phase solute transport through homogeneous soils. Water Resour Res 1985;21:808–20.
[66] Van Der Vost H. BI-CGSTAB: a fast and smoothly converging variant of BI-CG for the solution of nonsymmetric linear systems. SIAM J Sci Stat Comput 1992;13:631–44.
[67] Vayenas DV, Pavlou S, Lyberatos G. Development of a dynamic model describing nitritification and nitratification in trickling filters. Water Res 1997;31(5):1135–47.
[68] Wang J, Kitanidis PK. Analysis of macrodispersion through volume averaging: comparison with stochastic theory. Stoch Environ Res Risk Assess 1999;13(1–2):66–84.
[69] Whitaker S. Introduction to fluid mechanics. Malabar (FL, USA): R.E. Krieger; 1981.
[70] Whitaker S. The method of volume averaging. Dordrecht: Kluwer Academic Publishers; 1999.
[71] Wood BD, Whitaker S. Diffusion and reaction in biofilms. Chem Eng Sci 1998;53(3):397–425.
[72] Wood BD, Whitaker S. Cellular growth in biofilms. Biotechnol Bioeng 1999;64:656–70.
[73] Wood BD, Whitaker S. Multi-species diffusion and reaction in biofilms and cellular media. Chem Eng Sci 2000;55:3397–418.
[74] Wood BD, Dawson CN, Szecsody JE, Streile GP. Modeling contaminant transport and biodegradation in a layered porous media system. Water Resour Res 1994;30:1833–45.
[75] Wood BD, Quintard M, Whitaker S. Calculation of effective diffusivities for biofilms and tissues. Biotechnol Bioeng 2002;77(5):495–516.
[76] Wood BD, Cherblanc F, Quintard M, Whitaker S. Volume averaging for determining the effective dispersion tensor: closure using periodic unit cells and comparison with ensemble averaging. Water Resour Res 2003;39(8):1210. doi:10.1029/2002WR001723.
[77] Wood BD, Radakovich K, Golfier F. Effective reaction at a fluid–solid interface. Applications to biotransformation in porous media. Adv Water Resour 2007;30(6–7):1630–47. doi:10.1016/j.advwatres.2006.05.032.
[78] Wood BD, Golfier F, Quintard M. Dispersive transport in porous media with biofilms: local mass equilibrium in simple unit cells. Int J Environ Waste Manage, in press.
[79] Wood BD. Inertial effects on dispersion in porous media. Water Resour Res 2007;43:W12S16. doi:10.1029/2006WR005790.
[80] Wood BD. The role of scaling laws in upscaling. Adv Water Resour, in press. doi:10.1016/j.advwatres.2008.08.015.
[81] Young JC, McCarty PL. The anaerobic filter for waste treatment. J Water Pollut Contr Fed 1969;41:R160–73.